Astronomical pacing of Late Cretaceous third- and second-order sea-level sequences in the Foz do Amazonas Basin

Slah Boulila, Célia Brange, Alberto Machado Cruz, Jacques Laskar, Christian Gorini, Tadeu Dos Reis, Cleverson Guizan Silva

Astronomical pacing of Late Cretaceous third- and second-order sea-level sequences in the Foz do Amazonas Basin

Slah Boulila[1,2,*], Célia Brange[1,3], Alberto Machado Cruz[1,4], Jacques Laskar[2], Christian Gorini[1], Tadeu Dos Reis[4], and Cleverson Guizan Silva[5]

* corresponding author

Email adresses: slah.boulila@sorbonne-universite.fr (S. Boulila), celia.brange@gmail.com (C. Brange), albertomcruz88@gmail.com (A. Cruz), laskar@imcce.fr (J. Laskar), christian.gorini@sorbonne-universite.fr (C. Gorini), tadeu.reis@gmail.com (T. Dos Reis), cguizan@id.uff.br (C. G. Silva).

[1] Sorbonne Université, CNRS, Institut des Sciences de la Terre Paris, ISTeP, F-75005 Paris, France

[2] IMCCE, CNRS, Observatoire de Paris, PSL University, Sorbonne Université, 77 Avenue Denfert-Rochereau, 75014 Paris, France

[3] Institut Polytechnique UniLaSalle, 19 rue Pierre Waguet, B.P. 30313, 60026 Beauvais cedex, France

[4] Universidade do Estado do Rio de Janeiro, Faculdade de Oceanografia, Rua São Franscisco Xavier, 524, 4° andar, sala 4028, Maracanã, 20550900 - Rio de Janeiro, RJ – Brasil

[5] Universidade Federal Fluminense, Departamento de Geologia, Av. Gen. Milton Tavares de Souza s.n., Gragoatá – Niterói CEP: 24.210346

Abstract

Because of their relatively reduced tectonic influence, post-rift sedimentary successions have a propensity to preserve climatically-driven cyclicity over long durations. Here we present an integrated cyclostratigraphic and sequence stratigraphic study of the post-rift Limoeiro sedimentary Formation (Fm) of the Foz do Amazonas Basin (offshore Brazil), which spans the entire Late Cretaceous epoch (almost 35 Myr long). The principal goal of the present study is to decipher very long (multi-Myr) sedimentary cyclicities and their potential origin(s) in order to delineate the main controlling factors of post-rift sediment sequences and packages.

We used gamma-ray (GR) well-log data for cyclostratigarphy, and seismic data for sequence stratigraphy. Time-series analysis of GR data shows a rich series of Milankovitch frequency bands. In particular, long-period cyclicities (405 kyr, 2.4 Myr, 4.7 Myr and 9.5 Myr) are detected with high fidelity. Seismic and sequence stratigraphic interpretation shows a striking sea-level (SL) depositional sequence order, matching the 4.7 Myr orbital cyclicity inferred from cyclostratigraphy. Longer SL sequences interpreted in previous studies from the Limoeiro Fm closely match the 9.5 Myr GR related orbital cycles.

Thus, we infer that the post-rift Limoeiro Fm was deposited continuously under astronomical forcing over the Late Cretaceous epoch, resulting in an extraordinary record of direct base- and sea-level responses to Milankovitch climatic forcing, including longer (multi-Myr) periodicities. The 4.7 Myr orbital component is recorded for the first time in SL sedimentary proxies, thus allowing here to update SL hierarchical orders. We suggest that third-order, and second-order and suborders SL sequences were most likely paced by long-period astronomical cycles (2.4 Myr eccentricity, and 4.7 and 9.5 Myr orbital cycles, respectively.

Keywords: Cyclostratigraphy, sequence stratigraphy, climate, tectonics, Late Cretaceous, Foz do Amazonas Basin.

1. Introduction

Climate and tectonics are the main competing factors in the sedimentary systems, which together regulate base level in continents and sea level (SL) in oceans and seas. While climate change controls SL depositional sequences at shorter timescales (few tens kyr up to few Myr), in particular at Milankovitch cycle band (e.g., Strasser et al., 1999; Boulila et al., 2011), tectonic evolutions have been generally suggested to form SL depositional sequences at longer timescales (Myr to few hundreds Myr) because major plate tectonic motions occur at a very slow pace (Vail et al., 1977; Haq et al., 1987). As such, global SL (eustatic) sequences have been divided into different orders reflecting their amplitudes and timescales as well as their controlling factors, i.e. climate or tectonics (e.g., Vail et al., 1977; Haq et al., 1987, 1988; Hardenbol et al., 1998; Miller et al., 2005a; Simmons, 2012).

Precursor studies have shown the hierarchy of eustatic sequences from seismic data and well-log stratigraphy (Vail et al., 1977; Haq et al., 1987, 1988). In particular, Vail et al. (1977) divided these eustatic sequences temporally into six orders ranging from tens hundreds of millions years (first- and second-order) to tens of thousands years (sixth order). First- and second-order SL sequences were ascribed to tectono-eustatic changes in the global ocean volume, while fourth-, through sixth-order SL sequences were attributed to climate change within the Milankovitch (insolation) band. However, third-order SL sequences were interpreted as the result of climate or tectonic forcing (Vail et al., 1991; Cloetingh, 1988;

Strasser et al., 2000), while more recent studies have argued long-period (1.2 and 2.4 Myr) Milankovitch forcing of Cenozoic and Mesozoic third-order SL cycles (Boulila et al., 2011). A very recent study have proposed an updated SL sequence hierarchy and their potential controlling factors, based on time-series analysis of the Phanerozoic reference eustatic data (Boulila et al., 2018a).

Combined cyclostratigraphic and sequence stratigraphic studies increasingly show that the role of climate and SL changes in the formation of depositional sequences is more important, hence covering a wider frequency band (Boulila et al., 2011; 2018a). First attempts made to relate third-order (and lower) eustatic sequences to long-period 1.2 and 2.4 Myr (and longer) Milankovitch cycles were based on a comparison of eustatic sequence durations with orbital periodicities and/or on time-series analysis of compiled eustatic data (Boulila et al., 2011, 2018a).

Another more effective approach is to perform an integrated cyclostratigraphic and sequence stratigraphic study from a same sedimentary basin in order to decipher both SL sequences and astronomical cycles for a potential link. Previous studies were hampered by the lack of coupled climate and eustatic proxy data, or by the unavailability of very long climatic proxy record susceptible to register multi-Myr climate and SL variations (Boulila, 2019).

Here we present an integrated cyclostratigraphic and sequence (seismic) stratigraphic study on the Limoeiro sedimentary Formation (Fm) of the Foz do Amazonas Basin (offshore Brazil), which spans the entire Late Cretaceous epoch (34.5 Myr long, from 66 to 100.5 Ma, Gradstein et al., 2012). The main objective of the present study is to seek possible link between long-period (> 405 kyr) Milankovitch cycles inferred from cyclostratigraphy and SL depositional sequences inferred from seismic stratigraphy.

2. Geologic and stratigraphic settings

2.1. Geologic and stratigraphic setting of the Foz do Amazonas Basin

The Amazon River Mouth Basin (also called "*Foz do Amazonas*" basin) is located in the northwestern part of the Brazilian equatorial margin (Fig. SI-1). It covers an area of about 360000 km^2 (Silva et al., 1999). The Amazon Fan or Amazon Cone is situated in the center of the basin. It is one of the largest river-fed mud-rich submarine fan systems in the world, deposited over an area of 330000 km^2. It extends from the shelf break to 1100 km Northeast offshore, up to about 4.8 km water depth (Damuth et al., 1988).

The Brazilian Equatorial Margin history began during the rifting and opening of the Equatorial Atlantic Ocean, as a result of fragmentation and separation of northwestern

Gondwana (Fig. SI-2). According to Matos (2000), deformations associated with opening of the South Equatorial Atlantic started as early as the Jurassic-Triassic (225-145 Ma), although major rifting occurred too long later during late Barremian to late Albian (~120 to 105 Ma). These deformations were mostly linked to transforming motion that generated a series of complex marginal sedimentary basins, characterized by multiple phases of subsidence and different structural styles (Figs. 1 and SI-3, Matos, 2000). The resulting transform fracture zones correspond to structural lows as well as an area of deep grabens in the northwestern part of the basin (Fig. 1). The Offshore Amazon basin, located in the westernmost part of the the Equatorial Atlantic Ocean, is a particular basin of continental divergent passive margin (e.g. Brandão and Feijó, 1994; Moulin et al., 2010)

The stratigraphic evolution of the Foz do Amazonas Basin depositional sequences (Figs. 2 and 3). Two most recent publications providing the complete stratigraphy of the basin come from Petrobras oil & gas Company (Brandão and Feijó, 1994; Figueiredo et al., 2007). The pre-rift megasequence corresponds to the Calçoene Fm of Triassic-Jurassic age. The syn-rift megasequence corresponds to the Cassiporé and Codó Fms, and spans the Early Cretaceous epoch.

The post-rift megasequence encompasses the Limoeiro and Amapá Fms, spanning together the Late Cretaceous through the Middle Miocene. The Limoeiro Fm, which is the subject of the present study (detailed in Section 2.2), covers the Late Cretaceous epoch (Figueiredo et al., 2007). It is overlied by alternation of carbonates (Amapá Fm) and muddy deltaic sediments (Marajó and Travosas Fms) deposited during the Late Paleocene through the Middle Miocene. The present depositional system has started in the Late Miocene and contributed to building the Amazon Fan, which is the most prominent feature in the basin, called Pará Group's Stratigraphic Fms including Tucunaré, Piracuru and Orange Fms (Figs. 2 and 3).

2.2. Stratigraphic framework of the studied Limoeiro Fm

The Limoeiro Fm is a part of post-rift deposits, where its maximal thickness could reach 2.5 km in depocenters and tilted grabens created during the rifting (Brandão and Feijó, 1994). In the present study, we have focused on data from the area of deep grabens, located in the northwestern part of the basin (Figs. 1 and SI-3).

The transition between the Limoeiro Fm and the underlying Cassiporé Fm is marked by an angular unconformity between the tilted syn-rift strata and the sub-horizontal post-rift layers. The youngest post-rift layers are expressed in seismic data with moderate to strong amplitude reflectors, continuous sub-horizontal, and gradually thickening towards offshore. The upper boundary of the Limoeiro Fm was defined by the onset of the first carbonate layers of the overlying Amapá carbonate plateform Fm.

A potential source rock dated at around the Cenomanian-Turonian transition is about 500 to 1000 m thick below the Amazon fan (Cobbold et al., 2004), which was likely deposited under anoxic marine conditions (Cobbold et al., 2004; Mello et al., 1989, 1995).

Because of intense basin gravity tectonics, especially in the central part of the basin, Cenomanian-Holocene (100 Ma to present) deposits are affected by listric normal, thrust and strike-slip faults (Cobbold et al., 2004; Perovano et al., 2009; Reis et al., 2010, 2016). Such structural gravity-driven framework is rooted into three basal-detachment stratigraphic levels, pointed out on seismic data (Silva et al., 1999; Cobbold et al., 2004; Perovano et al., 2009; Reis et al., 2010, 2016): the older one, within the Limoeiro Fm dated at around 100 Ma, accomodates an inherited thrust-and-belt system; a more important one, dated at about 65 Ma, acts as a regional basal detachment of modern and more complex thrust-and-belt system, affecting both the carbonate platform and the Amazon-derived deposits; finally, the younger and less important detachment, at around 10.5 Ma, locally affects the central Amazon fan.

3. Material and methods

3.1. Gamma-ray well-log data and seismic stratigraphy

We used gamma-ray (GR) well-log data for cyclostratigraphy, and seismic data for sequence stratigraphy. GR indicates the amount of radioactive atomic nuclei of uranium, thorium, potassium, radium and radon in the rocks. GR has been successfully used as an indirect paleoclimatic proxy to characterize orbitally driven continental and marine sediments (e.g., Weedon et al., 2004; Wu et al., 2013). We have used GR data from the two wells APS-29-AP and APS-44-AP (hereafter wells 29 and 44 respectively, Fig. 1), which covers the whole Limoeiro Fm (Fig. 4). Resolution of GR data ranges from 15 to 20 cm, and their values are expressed in API (American Petroleum Institute) unit. In wells 29 and 44, GR data range from nearly 20 to 150 API, and the most important variations are mainly related to lithological changes from clays, siltstones and sandstones (Fig. 4).

The seismic dataset includes approximately 20,000 km of 2D multi-channel seismic data (made available by the Brazilian Navy and ANP-Brazilian Petroleum and Gas Agency) and two blocks of 3D multi-channel seismic data covering 3,800 km^2 (made available by CGG company).

Five 2D seismic lines useful for this study (Fig. SI-5) where only accessible as pictures and without numerical data, so they were just useful for having a larger view outside the 3D block, but they were not interpreted. The quality of these 2D multi-channel lines were not good compared to the 3D multi-channel seismic block (Fig. SI-5). The northwestern 3D seismic block (Fig. SI-5) also called BM-FZA-4/5 was acquired in 2007 by CGG. This PSTM (Pre-Stack Time Migration) survey covers 1700 km^2 of 60 fold 3D data. This survey is a medium good data knowing that the typical values of fold for modern 3D seismic data range from 10 to 120. The minimal vertical resolution around the Limoeiro Fm depth is 40 m.

Well logs were integrated to seismic dataset based on standard tools for 1D depth-to-travel time conversion available in Kingdom seismic interpretation software. Well 29 was tied to the available seismic data using a synthetic seismogram generated with sonic log (DT), density log (RHOB) and a seismic wavelet extracted from the seismic data (see Supplementary Fig. SI-6). Well 44 was tied to the available seismic data using check-shot data acquired in the well's drilling site (approximately one travel-time measurement every 60 measured meters).

3.2. Bio-lithostratigraphy and total organic carbon (TOC) data

The Limoeiro Fm in wells 29 and 44 was entirely recovered by the wireline log. The base of the formation corresponds to an angular unconformity between the syn-rift and post-rift deposits. Additional analyses to check this boundary were made using the seismic data. The top of the formation is the sharp contact with the overlying carbonate deposits.

The Limoeiro Fm is 800 m thick in Well 29, and 1476 m thick in Well 44. This difference in thickness is due to the more proximal position of Well 44 with respect to Well 29. The lithology in Well 29 is dominated by claystones and siltstones, while Well 44 is predominantly composed of claystones and sandstones (Fig. 4).

The Limoeiro Fm was assigned to the entire Late Cretaceous epoch (Figueiredo et al., 2007). However, the only available biostratigraphic data provide constraints on the age of its upper boundary, acquired from Well 1-APS-45B-AP (hereafter Well 45B, Fig. SI-7). This well was drilled down to the Maastrichtian, where a calcareous nannofossil biomarker (*Micula murus*) was found around the top of the Limoeiro Fm. Its first and last occurrences were detected around 20 meters before the end of Well 45B (Fig. SI-7), thus providing ages of approximately ~69 and ~66 Ma (Burnett 1998; Lees and Bown, 2005). The ~66 Ma age corresponds most likely to the top of the Limoeiro Fm (Fig. SI-7). Consequently, only the top of the Limoeiro Fm is relatively well dated by biostratigraphy.

Several geochemical data were acquired, but with low resolution. We have focused in this study on the Total Organic Carbon (TOC) data to potentially detect organic-rich stratigraphic levels associated with the Oceanic Anoxic Event 2 (OAE2, 'Bonarelli Level') of the Cenomanian-Turonian transition (e.g., Mello et al., 1989), and eventually the OAE1d ('Breistroffer Level') of the latest Albian. The 'Bonarelli' OAE2 has been documented worldwide (e.g., Schlanger and Jenkyns, 1976; Paul et al., 1999; Tsikos et al., 2004; Jenkyns, 2010; Jarvis et al., 2011). Also, the Breistroffer OAE1d has been recorded in several basins including the Atlantic and Pacific oceans (Wilson and Norris, 2001; Navarro-Ramirez et al., 2015).

Only Well 29 exhibits TOC data (Fig. 4), but with a variable sampling step, which ranges from 3 to 30 m. TOC data vary from 0.3 to 4.4 % with two distinguishable intervals of higher TOC values (> 3 %), one at around 4320 m depth and the other at around 4470 m depth. Interestingly, the sampling step at these two intervals is the smallest, thus providing the highest resolution of 3 m. We have explored these two intervals as potential records of OAE2 (e.g., Mello et al., 1989) and OAE1d (Section 5.2).

3.3. Methods

3.3.1. Time-series analysis

We used the multi-taper method (MTM) spectral analysis (Thomson, 1982) to detect sedimentary cyclicities in GR data. MTM spectra were conducted using three 2π tapers, together with the robust red noise test (Mann and Lees, 1996) as implemented in the R package 'astrochron' freeware (Meyers, 2014). Prior to spectral analysis, GR data were detrended using the weighted-average lowess method (Cleveland, 1979). We also used the gaussian filter (Paillard et al., 1996) to extract the recorded astronomical cycles.

Astronomical time calibration (or tuning) of the Mesozoic records is problematic because of the lack of accurate orbital solutions that can be used for tuning stratigraphy older than about 50–60 Ma (Laskar et al., 2004, 2011). Fortunately, there is one notable exception: the 405 kyr orbital eccentricity term, which can be estimated with high accuracy throughout the Mesozoic Era (Laskar et al., 2004).

As the analyzed interval (i.e., the Limoeiro Fm) covers approximately 35 Myr of Late Cretaceous, dramatic changes in the sedimentation rate have been observed. Additionally, lithostratigraphy of the two wells sometimes shows intervals with homogeneous lithology, and sometimes intervals with pronounced lithological changes (Fig. 4). For instance, the more proximal Well 44 shows, from the base of the Limoeiro Fm till depth ~3200 m, quasi-homogeneous lithology dominated by clays. However, the upper part of the Limoeiro Fm in Well 44 exhibits prominent alternations of clayey and sandy lithologies. Such differences in the lithology along each well strongly affects GR variations, with the more homogeneous intervals being characterized by lower amplitudes and intervals with contrasted lithologies by stronger amplitudes (Fig. 4).

To reduce the impact of the aforementioned factors on GR variations, i.e. the lithology and changes in sedimentation rate, we have conducted a cyclostratigraphic analysis per intervals in each well. The length of the selected intervals is not constant between the two wells and even within each well. It depends on the lithological change, and on the wavelengths of high- and low-frequency cyclicilies. Our approach was first to analyze short intervals to capture precession, obliquity and short eccentricity cycles, then analyze longer intervals to capture several 405 kyr eccentricity oscillations (Supplementary Information SII). We used frequency ratio method to infer to the statistically detected sedimentary cycles a Milankovitch astronomical origin (Section 4.1).

Finally, we focused on the wavelength related to the 405 kyr eccentricity component. We bandpass filtered it, tuned each analyzed interval to a pure 405 kyr periodic signal (Laskar et al. 2004), and assembled all the 405 kyr tuned intervals in order to merge and define an age model for each well, called floating timescale (e.g., Hinnov and Hilgen, 2012). The obtained 405 kyr floating timescale was then anchored to the age of onset of OAE2 (94.17 Ma, Batenburg et al., 2016), which corresponds to a maximum of a 405 kyr eccentricity cycle in La2011 astronomical model (Laskar et al., 2011). Finally, the 405 kyr GR cycle extremes were tied to the 405 kyr La2011 eccentricity cycles in order to obtain an absolute astronomical timescale.

We applied spectral analysis to the whole (405 kyr) GR calibrated Limoeiro Fm to seek very long-period Milankovitch cycles. In particular, the output 405 kyr tuned GR series could be examined for alignment of other, higher frequency terms associated with for e.g., the short (100 kyr) eccentricity, the lower frequency terms associated with g1-g5, s4-s3, g4-g3 (0.95, 1.2 and 2.4 Myr Cenozoic mean periods, see Table 1), with a special focus on the very longer orbital periods of 4.7 and 9 Myr (Boulila et al., 2012; Boulila, 2019). These longer periods will be potentially compared to SL depositional sequences inferred from seismic data.

3.3.2. Sequence and seismic stratigraphy

Well 29 presents a reference record in the Foz do Amazonas Basin, which was used to describe the sequence stratigraphic framework of the Limoeiro Fm (Fig. 2). Wells 29 and 44 are the only ones connected with seismic data, thus having the potential to realize a direct correlation between SL sequences inferred from seismic data and astroclimatic cycles inferred from GR data. In order to characterize the main horizons and identify major unconformities and sequence boundaries, the seismic interpretation was based on the analysis of seismic stratigraphic terminations. Their organization is related to the acoustic impedance contrast between genetically related strata, leading to the identification of sedimentary bodies within a stratigraphic sequence. We have used the Kingdom software, which is dedicated to correlate the main horizons across the northwestern 3D block between Well 44 (north of the block) and Well 29 (south of the block). On the overall progradation of the Limoeiro seismic megasequence, major uncomformities have been identified based on the classical seismic stratigraphy (e.g., Vail et al., 1977; Haq et al., 1987, 1988; Christie-Blick et al., 1990; Miller et al., 2018; Catuneanu, 2019). The recognition of major stratigraphic surfaces on the seismic data is based on stratigraphic principles as defined by Vail et al. (1977), with mainly Maximum Flooding Surfaces (MFS) characterized by downlap surfaces and Sequence Boundaries (SB) identified by both onlap and truncation or erosional surfaces. Projection of MFS and SB into borehole logs were performed using synthetic seismograms (created using check shots and sonic and density logs, see Supplementary Fig. SI-6).

4. Results

4.1. Cyclostratigraphy

Power spectra of the Limoeiro Fm in depth domain in Well 29 shows two strong peaks of 240 and 56 m (Fig. 5A). Power spectra per intervals highlight additional peaks, in particular two peak bands in the order of 10 and 2.5 m (Fig. SII-1; Fig. 5A). Frequency ratio method indicates short (100 kyr), 405 kyr (g2-g5), and 2.4 Myr g4-g3) eccentricity periods for respectively peaks 2.5, 10 and 56 m. Power spectra in the 405 kyr time domain (see 'Methods') calibrates the 240 m peak to a period of 9.7 Myr, the 56 m peak to a period of 2.4 Myr, the peaks around 2.5 m to periods around 100 kyr (Fig. 5B), thus reciprocally matching the eccentricity components. Two other peaks of 30 and 23 m are calibrated to 1.3 and 1.0 Myr respectively, thus they may correspond to s4-s3 and g1-g5 orbital frequencies (Table 1).

Power spectra of the Limoeiro Fm in Well 44 shows two strong peaks of 383 and 203 m (Fig. 5C). Power spectra per intervals highlight several additional peaks of wavelengths of 96, 50, 17, 7.5 and 4 m (Fig. SII-2; Fig. 5C). Frequency ratio method conjointly with the g2-g5 orbital tuning indicates that the shortest 4 m wavelength may correspond to the short eccentricity, the 7.5 m to s3-s6 (173 kyr, see Boulila et al., 2018b), the 17 m to g2-g5 (405 kyr target), the 50 m to s4-s3 (1.2 Myr), the 96 m to g4-g3 (2.4 Myr), and the 203 and 383 m to 4.7 and 9.5 Myr orbital periods respectively (see also Table 1).

The 405 kyr (g2-g5) tuning in the two wells (Figs. 6 and 7) yields the same duration of ~35 Myr (equivalent to eighty six g2-g5 cycles) for the Limoeiro Fm (Fig. 8). Evaluation of orbital age models is discussed in Section 4.2.

The recorded orbital cycles in GR data sometimes match the lithology, but sometimes they do not. For instance, in apparently homogeneous claystone or sandstone intervals, significant orbitally controlled GR fluctuations could be observed (Figs. 6 and 7). Also, there is no preferentially expressed orbital parameter within the lithology. Dominant cyclic (alternating) lithologies could sometimes match the short eccentricity, and sometimes the long 405 kyr eccentricity (Fig. SII-2).

4.2. Sequence and seismic stratigraphy

The top and the base of the Limoeiro Fm are marked by reflectors with high amplitude, which can be followed from north to south of the 3D seismic block.

Seismic Inline 3273 crosses exactly at the level of Well 29. With the maximal vertical resolution of 40 m, Inline 3273 shows 20 reflectors within the Limoeiro Fm equivalent interval, but these reflectors could not be extrapolated neither till Well 29 site nor till Well 44 site along the crosslines or the arbitrary lines.

The log and seismic calibration was derived from inline 1454, which was tied to Well 44 located in the northern part of the 3D seismic block. Seismic resolution is not very good (about 40 m); however, the studied interval is thick enough (1476 m thick in Well 44) to identify the major depositional sequences. Picking is based on stratigraphic principles, with mainly MFS characterized by downlap surfaces, and SB by both onlap and truncation or erosional surfaces. Taking into account the location of Well 44, which is relatively proximal, we found mainly systems tracts related to transgressive and regressive phases (Figs. 9 and 10). However, when moving seaward we can observe on the seismic data the development of main lowstand systems tracts (LST) which are rooted on the main sequence boundaries. As a result, we picked seven MFS and six SB. Thus, six well-defined sequences in Well 44 (interval from about 2200 m till about 3250 m) were the subject of a potential correlation with long-period astroclimatic cycles inferred from GR data.

The identification of LST is based on the position of marine onlaps on the paleoslopes (LST in orange-shaded areas in Fig. 9). The erosional uncomformities (red lines in Fig. 9, subareal uncomformities on paleoplatforms *sensu* Catuneanu, 2006), with their correlative conformities basinward, were placed at the base of the indentified LST. They have been interpreted as major SB *sensu* Posamentier and Vail (1988). Back step geometries characterize the transgressive intervals (thickening toward the continent). The green surfaces on top of these intervals are materializing the downlap surfaces. More generally, these green surfaces correspond to the turning point between retrogradation (back step geometries on the seismic data, with a thickening toward the continent) to the progradation (downlaps), and correspond to maximum floodings.

All seismic units above Sequences boundaries (SB, *sensu* Vail et al., 1977) show poorly stratified series basinward, indicating that unstable shelf edges led to mass wasting of unconsolidated sediments. Some of the shelf edges also show listric detachments (see Fig. 9). Consequently, the shelf edge presents chaotic internal geometries, indicating that these collapses originated mass transport deposits (MTDs) to the deeper basin. Abrupt terminations of the topset beds, indicate that mass movement of material to the deeper basin has been completed prior to subsequent flooding. Discussion about the nature of LST is beyond the scope of this paper, however, we infer that mass-transport processes described for Quaternary strata by several authors (e.g., Damuth and Kumar, 1975; Damuth and Embley, 1981; Maslin et al., 1998), and for older Pliocene sediments (see also Reis et al., 2010; Silva et al., 2010; Gorini et al 2013) may have been also operative since the early post-rift evolution of the margin and could be part of the lowstand deposits.

5. Discussion

5.1. Evaluation of g2-g5 orbital age models

The Limoeiro Fm was poorly dated in the literature. It was roughly attributed to the entire Late Cretaceous epoch (Figueiredo et al., 2007) with only one chronostratigraphic age control (~66 Ma) at its upper boundary, inferred from calcareous nannofosil biostratigraphy (Section 3.2).

The absolute g2-g5 age model in Well 29 depends on the anchoring age point at the onset of OAE2 (94.17 Ma, Batenburg et al., 2016) assuming that the start of TOC peak, at 4320 m depth, records the onset of this event. Such age model provides an age of 66.472 Ma for the top of Limoeiro Fm (Fig. 6). This age is older than the biostratigraphically inferred age of ~66 Ma, by only one g2-g5 equivalent cycle. In addition, the g2-g5 age model in Well 29 yields an age of 100.35 Ma for the lower TOC peak (4470 m depth) that we suspect to document the OAE1d (Section 3.2). The duration between the starts of the two TOC peaks assumed to record the OAE2 and OAE1d is 6.180 Myr (from 100.35 to 94.17 Ma), which is close to that reported in the literature (e.g., ~6 Myr, Sprovieri et al., 2013).

Well 44 provides additional constraints on g2-g5 age model. Interestingly, the Limoeiro Fm encompasses the same number of g2-g5 cycles in the two wells (i.e., 86 cycles, Figs. 7 and 8). Because of the absence of TOC data in Well 44, g2-g5 floating timescale in this well was anchored at the base of a GR peak (3650 m depth), which is correlatable to a GR peak in Well 29, assumed to match the OAE1d (100.35 Ma in Well 29). The resulting absolute g2-g5 age model in Well 44 provides an age of 66.646 Ma for the top of the Limoeiro Fm, which is only 0.174 Myr older than the 66.472 Ma astronomical age in Well 29. Furthermore, the base of a very strong, well-defined GR peak within a clayey interval in Well 44 (at 3395 m depth) has surprisingly an age of 94.10 Ma. We suspect that this strong peak in Well 44 may match the equivalent OAE2 interval in Well 29 (Fig. 8).

In summary, three remarkable age points from g2-g5 age model in Well 29, which is a reference well in the Foz do Amazonas Basin (see above), could be considered in future studies are: (1) the top of the Limoeiro Fm at ~66.472 Ma, (2) the start of the older TOC peak at ~100.35 Ma matching the OAE1d and nearly the base of the Limoeiro Fm, and (3) the start of the younger TOC peak at ~94.17 Ma, corresponding to the onset of OAE2.

Although the consistency in age models between the cyclostratigraphically calibrated wells 29 and 44 and previous studies of the Limoeiro Fm (e.g., Figueiredo et al., 2007), the only available biostratigraphic age of the upper limit of the Limoeiro Fm (Supplementary Fig. SI-7) may weaken the potential of g2-g5 age models for use in future studies. Biostratigraphic age control is of paramount importance in the generation of astronomical timescales (ATS), because it is an independant approach on which the ATS should be built (e.g., Hinnov and Hilgen, 2012). However, in the absence of accurate ages from biostratigraphy (or integrated biochronostratigraphy), g2-g5 orbital tuning has been used with success for Mesozoic and Cenozoic cyclostratigraphy (e.g., Boulila et al., 2008, 2010; Hinnov and Hilgen, 2012 ; Liu et al., 2018). The identification of 405 kyr (g2-g5) eccentricity cycle could be successfully fulfilled using frequency ratio method (e.g., Huang et al., 1992; Mayer and Appel, 1999; Boulila et al., 2008 their table 1; Hinnov and Hilgen, 2012). Tuning wells 29 and 44 to a pure 405 kyr periodicity (Laskar et al., 2011) allows to correct considerable variations in sedimentation rates, and the alignement of other, higher and lower frequency terms (Section 4.1). Thickness of the 405 kyr related eccentricity cycles ranges from 7 to 11.8 m in Well 29, and from 8.7 to 24.5 m in Well 44 (Section 4.1 and Supplementary information II). The g2-g5 age models calibrate wavelengths to temporal periods, which are very close to those predicted in the astronomical models. In particular, shorter wavelengths related to the short eccentricity cycles are calibrated to periods around 100 kyr (Figs. 5B,D). The longer wavelengths, related to g4-g3 eccentricity component, are calibrated to a period of 2.4 Myr (Fig. 5B). Thus, the 405 kyr tuning further supports cyclostratigraphic interpretations inferred from frequency ratio method (Section 4.1). Accordingly, we used the potential of g2-g5 age models to explore long-period cyclicities and their possible impact on SL changes.

5.2. Astronomical origin of the 4.7 Myr cycles

The strong expression of the 4.7 Myr orbital cyclicity in SL record leads us to discuss its possible origin in more detail. A ~4.7 Myr cyclicity can be directly retrieved in the eccentricity time series as the libration period of the resonant argument θ = 2(g4 – g3) − (s4 – s3), where g3, g4 are related to the precession of the perihelions of the Earth and Mars, and s3, s4 are related to the precession of the nodes of the same planets (Laskar, 1990). It could also be retrieved from the obliquity time series (Supplementary information III). More precisely, it could be obtained when one considers only the proper modes of the secular frequencies in the precession of perihelia and nodes of the inner planets (Fig. SIII-1). The ~2.4 and ~4.7 Myr are present either in the precession of perihelia or in the precession of nodes, but with different phase relationships. They are in phase at the ~4.7 Myr band, but antiphased at the ~2.4 Myr band (Fig. SIII-1).

In fact, Laskar (1990) highlighted a fundamental libration period of ~4.7 Myr for θ (so-called here as Pθ and the correspondant frequency as Fθ). This libration oscillation corresponds to the oscillations of a pendulum, which is close to what occurs in case of resonances, when a combination of frequencies becomes null (here 2(g4 – g3) − (s4 – s3) = 0). The four frequencies g3, g4, s3, s4 are no longer independent and a new frequency, the libration frequency, appears as a new independent frequency (Fθ = 0.28 arcsec/yr, Pθ ≈ 4.7 Myr). Here, the frequency of libration Fθ is itself in rational ratio with 'g4 – g3' (2Fθ = g4 – g3 = 0.58 arcsec/yr ≈ 2.4 Myr) as was observed in Laskar (1990). Amplitude harmonic analysis of variations of the resonant argument θ (Fig. 11) shows a strongest peak at ~4.7 Myr, which represents the fundamental libration frequency Fθ. Then, harmonics of Fθ (i.e., 2Fθ, 3Fθ, 4Fθ, 5Fθ, 6Fθ, 7Fθ) appear in the spectrum, with a dominance of odd mode resonance frequencies (3Fθ, 5Fθ, 7Fθ). A ~1.6 Myr period appears that can be related to a combination of Fθ, i.e., 3Fθ (0.84 arcsec/yr ≈ 1.6 Myr). This periodicity, which also modulates the climatic precession at the two terms '$p+g_4$' and '$p+g_3$- Fθ' (Table 1), was recently detected in the Cenozoic climatic record (Boulila, 2019). The ~4.7 Myr cyclicity in the eccentricity time series is also modulating the climatic precession at the two frequencies '$p+g_3$' and '$p+g_3$ +Fθ' (Table 1). Such long-term cyclicity has been detected in the sedimentary carbon-cycle proxies (Boulila et al., 2012; Spovieri et al., 2013), and may have an impact on SL change (Section 4.3).

5.3. Third- and second-order SL sequences: durations and causal mechanisms

Precursor studies have considered the important role of sea-level changes in the sedimentary records, and thus proposed an hierarchical link among different orders of SL depositional sequences (e.g., Vail et al., 1977; Haq et al., 1987, 1988). This hierarchical link is based on magnitude and duration of SL sequences. While the quantification of magnitude (or amplitude) of SL fluctuations has received controversial interpretations (Vail et al., 1977; Haq et al., 1987; Miller et al., 2005; Kominz et al., 2008; Müller et al., 2008), assessement of timing and duration of SL sequences has generally been agreeable among researchers (e.g., Haq et al., 1987; Miller et al., 2005). Although amplitude of SL oscillations is a fundamental criterion for sequence order determination (e.g., Vail et al., 1977), studies based on timing and duration of Mesozoic-Cenozoic SL sequences yield strong correlation between third-order SL sequences and long-period orbital cycles (Boulila et al., 2011).

Here we focus on durations of both third- and second-order SL sequences and their potential link with long-period astronomical cycles. Integrated cyclostratigtraphic and sequence stratigraphic study of the Limoeiro Fm hints at a connection between orbital forcing and SL change at these two orders (Sections 4.1 and 4.2). Seismically mapped depositional sequences have been considered to reflect SL fluctuations (e.g., Vail et al., 1977; Haq et al., 1987, 1988; Christie-Blick et al., 1990; Miller et al., 2018; Catuneanu, 2019). In particular, prominent SL sequences, detected seismically in the Limoeiro Fm, closely match the 4.7 Myr orbital cycles inferred from GR cyclostratigraphy (Figs. 9 and 10). Longer SL sequences were previously interpreted in the Limoeiro Fm (Brandão and Feijó, 1994; Figueiredo et al., 2007), and these sequences closely match the 9.5 Myr orbital cycles inferred from GR cyclostratigraphy (Fig. 10).

The 9.5 Myr cycles were attributed to shorter second-suborder SL sequences (Haq et al., 1987; discussed in Boulila et al., 2018a). However, the 4.7 Myr orbital cycle band has never been discussed in depth in SL proxies. It was evoked in Toarcian SL sequences (Boulila et al., 2014 their figure S6), but discussed in more detail in Cenozoic carbon-cycle data (Boulila et al., 2012, see their figures S2 and S4), and more recently in temperature proxy data (benthic $\delta^{18}O$) (Boulila, 2019). The 4.7 Myr orbital cyclicity is prominent in SL record (Section 4.2), thus it is used to update SL sequence hierarchy (Table 2).

Third-order sequences match 1.2 Myr (s4-s3) obliquity in icehouses and 2.4 Myr (g4-g3) eccentricity in greenhouses, while fourth-order sequences were interpreted to reflect 405 kyr eccentricity cycle (Boulila et al., 2011, 2014). Neither the 2.4 Myr (third-order) nor the 405 kyr (fourth-order, Boulila et al., 2011) eccentricity cycles are seismically captured in this study, likely because of low resolution of seismic data. However, high-resolution cyclostratigraphic study shows evidence for a strong expression of 405 kyr and 2.4 Myr eccentricity in the Late Cretaceous greenhouse (Fig. SII-3), which most likely correspond to fourth- and third-order SL sequences, respectively.

In a recent study (Boulila et al., 2018a), SL orders and suborders were updated on the basis of time-series analysis of the Phanerozoic SL data. Indeed, second-order SL sequences have two suborders: 9.5 and 36 Myr (Boulila et al., 2018a). Here we add to them another suborder, which corresponds to 4.7 Myr orbital band (Table 2). Thus, second-order SL sequences possesses now three suborders: the shortest is the 4.7 Myr band, the middle one corresponds to the 9.5 Myr band, and the longest one match the 36 Myr cycle band. The 4.7 and 9.5 Myr SL cyclicities have most likely a Milankovitch astronomical origin (Section 4.2; Boulila et al., 2012). The 36 Myr SL cycle has been ascribed to another dimension of astronomical forcing (vertical motion of the solar system) and/or to tectonics (Boulila et al., 2018a) (Section 5.4). It is worthwhile that another 16-18 Myr cycle band, hence falling into the second-order timescales (Table 2), could be barely seen in the analyzed GR records, because the signals are too short to determine its actual period. There are potentially two 16-18 Myr oscillations (Fig. 10). Nevertheless, such cyclicity could be retrieved from compiled SL data of the past 110 Ma (Fig. SIV-1) (see also figure 2 of Boulila, 2019).

The hierarchical link between durations of third-order, and second-order and suborders SL sequences (1.2, 2.4, 4.7, 9.5, 18, 36 Myr) leads us to reassess the role of astronomical forcing in the formation of SL depositional sequences. Although such link hints at a connection between SL and astronomically driven climates, global tectonic forcing on SL change, at 9.5 Myr band and longer, could not be excluded (Section 5.4).

Even at shorter timescales, tectonics undoubtedly interferes within the sedimentary SL archive. However, the principal cause that emerges in the SL record at the million to multi-million year timescale is seemingly the astro-climatically driven signal.

5.4. Tectonic versus climate control of sea-level changes

Eustasy or global mean sea-level (e.g., Haq et al., 1987; Myers and Milton, 1996; Miller et al., 2018) has received a particular interest in several geoscience domains because of its numerous potential implications for petroleum exploration, biogeochemocal cycles, biomass evolutions and turnovers, and the development of the geological time scales (see Simmons, 2012; Simmons et al., in press for extensive reviews). Thus, the study of eustatic drivers is of paramount importance to better understanding the related geological processes. In particular, assessment of the duration of eustatic sequences can help to decipher their causal mechanisms (Table 2).

Although long-term (100 to several 100s of Myr) eustatic variations have generally been seen as the result of changes in the global ocean volume induced by plate tectonic motions, outstanding questions remain on the cause of shorter term eustatic changes of few Myr to several 10s of Myr.

For instance, paleo-tectonic reconstructions show a correlation between major tectonic phases and eustatic sequences at the Wilson-Cycle scale, of duration of 250-300 Myr (Cogné et al., 2006). However, the pronounced 36 Myr eustatic cyclicity observed throughout the Phanerozoic eon has not found its equivalent in the tectonic variations, possibly because the absence of accurate paleo-tectonic reconstructions (Boulila et al., 2018). Thus, another alternative cause from the vertical motion of the solar system in the galaxy via the incident cosmic rays has been equally suggested, though the impact of cosmic rays on climate is a debated subject (Table 2).

Milankovitch orbital forcing of insolation driven climate has been widely argued (Hays et al., 1976; Hinnov, 2015; Hilgen, 2010), and today there are increasing evidences for Milankovitch control of climate, carbon-cycle and sea-level at Myr to multi-Myr timescales (Boulila et al., 2011 and references therein; Boulila et al., 2012; Sprovieri et al., 2013; Boulila, 2019).

The 1.2 Myr obliquity and 2.4 Myr eccentricity cycles have been recognized in both the astronomical and geological variations (e.g., Laskar et al., 2004; Pälike et al., 2004, 2006), and their impacts on sea-level sequences have been argued (see Boulila et al., 2011 for an extended review). The 4.7 Myr orbital cyclicity has less been identified in the astronomical and geological variations (Boulila et al., 2012, 2014; Sprovieri et al., 2013; Boulila, 2019). The 4.7 Myr has been detected in both the eccentricity and obliquity signals (Boulila et al., 2012) (see Section 5.2 for its precise origin). The 9.5 Myr orbital cycle has been retrieved for the first time from the modulation of both the eccentricity and obliquity signals (Boulila et al., 2012; Boulila, 2019). Its record in the geological archives has been successfully retrieved from deep-sea (benthic foraminifera) stable carbon and oxygen isotopes (Boulila et al., 2012; Boulila, 2019).

At ten to tens of Myr timescales, geodynamic modeling has shown different cyclicities of ~25 Myr for the spreading and production rates of oceanic ridges (Cogné and Humler, 2006), and of 25-50 Myr and 10-15 Myr for arc magmatism (DeCelles et al., 2009; Wolfram et al., 2019), although some studies have pointed to the fractal nature of arc magmatism (e.g., de Silva et al., 2015). Interestingly, extended synthetic observations throughout the Phanerozoic eon from the Canadian High Arctic show 10 Myr pseudo-periodic sedimentary sequences correlated to tectonic episodes (Embry et al., 2019). Such study indicates that tectonics from uplift and subsidence was responsible for the formation of depositional sequences of durations ranging from 4 to 17 Myr. These durations overlap with the 4.7 and 9.5 Myr orbital cycles, leading us to reassess the importance of a coupled climate and tectonics effect that could play a role in SL changes at ten to tens of Myr timescales. Intriguing match between variations in external (climate) and Earth's interior processes has been observed at shorter (Kutterolf et al., 2012; Crowley et al., 2015; Huybers and Langmuir, 2009) and longer (Boulila, 2019) timescales, pointing to potential feedback responses of Earth's interior dynamics to astronomically driven climate and Earth's surface processes (see also discussion in Boulila, 2019). For instance, orbitally paced glacial cycles have been correlated to oceanic crust production (Crowley et al., 2015).

5.5. Sea-level drivers in the Late Cretaceous "greenhouse"

The Late Cretaceous represents one of the warmest epochs of the past 150 Ma, with extreme greenhouse conditions culminating at the Cenomanian-Turonian Transition (e.g., Friedrich et al., 2012; Huber et al., 2018). Because there is no direct sedimentary evidence for polar ice caps, Earth has long been considered as ice free during the Late Cretaceous, in addition to the highest sea levels (SL) that this epoch documents (e.g., Haq et al., 1987; Haq, 2014; Miller et al., 2005a).

Despite the extreme warmth and highest SL conditions, Earth's climate witnessed severe, short-lived cooling events, coeval to prominent SL drops (Haq and Huber, 2016; Galeotti et al., 2009). These climatic coolings and SL falls have been argued worldwide on the basis of stable oxygen isotopes and sedimentological proxy data (e.g., Haq et al., 1987; Stoll and Schrag, 2000; Bornemann et al., 2008). Nevertheless, the record of prominent SL fluctuations (ca. 20 to 110 m, e.g., Haq, 2014) during the so-called ice-free Late Cretaceous epoch has generated an outstanding debate since the 1980's, regarding the existence (or not) of ice sheets on Earth, that may explain these rapid sea-level falls via glacio-eustasy (e.g., Matthews, 1984; Stoll and Schrag, 1996, 2000; Huber et al., 2002; Miller et al., 2005b; Bornemann et al., 2008; Boulila et al., 2011; MacLeod et al., 2013, among others).

Other causal mechanisms of short-term (e.g., Myr to multi-Myr) SL changes during the Cretaceous have been suggested on the basis of changes in the aquifer water volume and groundwater storages, i.e. aquifer-eustasy (Jacobs and Sahagian, 1993) or thermal expansion and contraction of seawater column i.e., thermo-eustasy (Gornitz et al., 1992; Schulz and Schäfer-Neth, 1998). However, such mechanisms could generate only few to tens of meters of SL oscillation (not more than 40 m). The aquifer-eustasy hypothesis has been recently resumed to explain Cretaceous SL changes (Wendler et al., 2016; Wagreich et al., 2014; Sames et al., 2016). Yet, such driver still could not explain the important sea-level fluctuations observed, for example, during the Turonian Stage (Haq et al., 1987; Haq, 2014; Haq and Huber, 2016), keeping glacio-eustasy the most plausible candidate (e.g., Miller et al., 2005b; Boulila et al., 2011; Ray et al., 2019; see also discussion in Simmons et al., in press).

The above discussed eustatic drivers (thermo-eustasy, aquifer-eustasy and glacio-eustasy) are all sensitive to orbitally forced climate. The 4.7 and 9.5 Myr orbital cycles recorded in SL data (Sections 5.2 and 5.3) are also documented in deep-sea (benthic foraminifera) stable carbon and oxygen isotopes, $\delta^{13}C$ and $\delta^{18}O$ (Boulila et al., 2012; Boulila, 2019). Although the resolution of the Late Cretaceous isotopic data is low compared to that in the Cenozoic, spectral analysis and filtering show evidence for 4.7 and 9.5 Myr cyclicities in benthic $\delta^{18}O$ climate record along the past 100 Ma (Boulila, 2019 his Figs. 1 and 2).

6. Conclusions

Integrated cyclostratigraphic and sequence stratigraphic study of the Late Cretaceous Limoeiro Fm in the Foz do Amazonas Basin (offshore Brazil) allowed the detection of a rich series of Milankovitch astronomical frequencies (100 kyr, 405 kyr, 2.4 Myr, 4.7 Myr and 9.5 Myr) together with a potential link between third- and second-order SL sequences, and long-period orbital cycles.

Cyclostratigraphy was performed on gamma-ray (GR) well-log data in two wells: Well 44 dominated by deltaic deposits and Well 29 dominated by deltaic to distal marine deposits.

Time-series analysis of GR data shows similar Milankovitch cycle hierarchy in the two wells, but a notable difference in amplitudes of the recorded cycles.

Long-period Milankovitch cyclicities (405 kyr, 2.4 Myr, 4.7 Myr and 9.5 Myr) were detected with high fidelity in the two sites. The 405 kyr stable eccentricity cycle permits to realize floating timescales for the two sites, and provides strong constraints on longer periods of Milankovitch orbital forcing.

The 2.4 and 9.5 Myr cyclicities dominate in Well 29, while 4.7 and 9.5 Myr cyclicities dominate in Well 44. We relate such differential orbital expression to different lithologies between the two wells, one dominated by clays and silts (Well 29) and the other by clays and sands (Well 44).

Sequence stratigraphy was based on seismic data especially those covering Well 44 because its location within a 3D seismic block conjointly with the good quality of reflectors. The seismically mapped strong SL sequences closely match the 4.7 Myr orbital cycles inferred from GR cyclostratigraphy. In addition, longer SL sequences were previously interpreted in the Limoeiro Fm, and correspond to the 9.5 Myr orbital cycles detected in GR data. The cyclostratigraphically detected orbital periods (405 kyr and 2.4 Myr), previously ascribed to fourth- and third-order SL sequences, respectively, were not seismically captured likely because of the low resolution of seismic data.

Accordingly, correlation of SL seismic sequences (fourth- to second-order) and long-period Milankovitch cycles suggests important contribution of astronomical forcing to the formation of SL depositional sequences. Fourth- and third-order SL sequences match respectively 405 kyr and 2.4 Myr eccentricity cycles. Shorter second-order and suborder sequences correlate to 4.7 and 9.5 Myr orbital cycles.

We hypothesize that even if teconics may interfere at Myr to multi-Myr frequency bands, the astroclimate signal strongly dominates and emerges in the sedimentary record at multi-Myr timescales. Thus, our finding reassesses more important role to climate forcing in SL sequences to the detriment of tectonics.

Acknowledgments

This study uses seismic and well-log data of the project IODP-CAPES "*Evolução estratigráfica e estrutural da bacia da Foz do Amazonas: acoplamento entre processos sedimentares, gravitacionais e de migração de fluidos*" sponsored By CAPES (Coordination for the Improvement of Higher Level Education- Brazil). We greatly thank Agência Nacional do Petróleo, Gás Natural e Biocombustíveis (ANP) that provided seismic and well-log data to Universidade Federal Fluminense (UFF, Brazil) and Universidade do Estado de Rio de Janeiro (UERJ, Brazil). Our special thanks are also due to CGG for providing 3D seismic grid to Institut des Sciences de la Terre Paris (ISTeP, Sorbonne Université, CNRS, France). Slah Boulila and Jacques Laskar were supported by French ANR Project AstroMeso. Alberto M. Cruz was supported by IODP-CAPES project grant No. 0558/2015. Antonio Tadeu dos Reis and Cleverson Guizan Silva received research grant No. 313086/2017-6 and No. 308164/2015-6 from the Brazilian National Research Council (CNPq). We are grateful to Editor Massimo Zecchin, and thank the two reviewers for very helpful reviews that led to important revisions of our manuscript.

References

Baker, P., Silva, C., Fritz, S., Reis, T., 2015. Deep drilling of the Amazon continental margin: The evolution of Cenozoic neotropical biodiversity, climate, and oceanography. IODP Proposal., https://docs.iodp.org/Proposal_Cover_Sheets/859-Full2_Baker_cover.pdf.

Batenburg, S.J., Vleeschouwer, D.D., Sprovieri, M., Hilgen, F.J., Gale, A.S., Singer, B.S., Koeberl, C., Coccioni, R., Claeys, P., Montanari, A., 2016. Orbital control on the timing of oceanic anoxia in the Late Cretaceous. Clim. Past Discuss. https://doi.org/10.5194/cp-2015-182.

Brandão, J.A.S.L., Feijó, F.J., 1994. Bacia da Foz do Amazonas: Boletim de Geociências da Petrobras, 8, 1, p. 91–99.

Bornemann, A., Norris, R.D., Friedrich, O., Beckmann, B., Schouten, S., Damsté, J.S.S., Vogel, J., Hofmann, P., Wagner, T., 2008. Isotopic evidence for glaciation during the Cretaceous Supergreenhouse. Science 319, 189–192.

Boulila, S., Galbrun, B., Hinnov, L.A., Collin, P.Y., Ogg, J.G., Fortwengler, D., Marchand, D., 2010. Milankovitch and sub-Milankovitch forcing of the Oxfordian (Late Jurassic) Terres Noires Formation (SE France) and global implications. Basin Research 22, 717−732.

Boulila, S., Galbrun, B., Huret, E., Hinnov, L.A., Rouget, I., Gardin, S., Bartolini, A., 2014. Astronomical calibration of the Toarcian Stage: implications for sequence stratigraphy and duration of the early Toarcian OAE. Earth Planet. Sci. Lett. 386, 98–111.

Boulila, S., Galbrun, B., Laskar, J., Pälike, H., 2012. A ~9 Myr cycle in Cenozoic $\delta^{13}C$ record and long-term orbital eccentricity modulation. Is there a link? Earth Planet. Sci. Lett. 317-318, 273–281.

Boulila, S., Galbrun, B., Miller, K.G., Pekar, S.F., Browning, J.V., Laskar, J., Wright, J.D., 2011. On the origin of Cenozoic and Mesozoic “third-order” eustatic sequences. Earth-Sci. Rev.109, 94–112.

Boulila, S., Hinnov, L.A., Huret, E., Collin, P.Y., Galbrun, B., Fortwengler, D., Marchand, D., Thierry, J., 2008. Astronomical calibration of the Early Oxfordian (Vocontian and Paris basins, France): consequences of revising the Late Jurassic time scale. Earth Planet. Sci. Lett. 276, 40−51.

Boulila, S., Laskar, J., Haq, B.U., Galbrun, B., Hara, N., 2018a. Long-term cyclicities in Phanerozoic sea-level sedimentary record and their potential drivers. Glob. Planet. Ch. 165, 128–136.

Boulila, S., Vahlenkamp, M., De Vleeschouwer, D., Laskar, J., Yamamoto, Y., Pälike, H., Kirtland Turner, S., Sexton, P.F., Cameron, A., 2018b. Towards a robust and consistent middle Eocene astronomical timescale. Earth Planet. Sci. Lett.486, 94–107.

Boulila, S., 2019. Coupling between Grand cycles and Events in Earth's climate during the past 115 million years. Scientific Reports, doi: 10.1038/s41598-018-36509-7.

Burnett, J.A. 1998. Upper Cretaceous. In P.R. Bown (Ed.), Calcareous Nannofossil Biostratigraphy. British Micropaleontology Society Publications Series, Kluwer Academic Publishers, London, p. 132–199.

Catuneanu, O., 2006. Principles of Sequence Stratigraphy. Elsevier, Amsterdam, 375p.

Catuneanu, O., 2019. Model-independent sequence stratigraphy. Earth-Science Reviews 188, 312–388.

Christie-Blick, N., Mountain, G.S., Miller, K.G. 1990. Seismic stratigraphy: record of sea-level change. In: Revelle, R. (Ed.) Sea-level change, National Research Council, Studies in Geophysics, National Academy Press, 116–140.

Cleveland, W.S., 1979. Robust locally weighted regression and smoothing scatter plots. J. Am. Stat. Assoc. 74, 829–836.

Cloetingh, S., 1988. Intraplate stresses: a tectonic cause for third-order cycles in apparent sea level? SEPM Spec. Publ. 42, 19–29.

Cobbold, P.R., Mourgues, R. and Boyd, K., 2004. Mechanism of thin-skinned detachment in the Amazon Fan: Assessing the importance of fluid overpressure and hydrocarbon generation. Marine and Petroleum Geology 21, 1013–1025.

Cogné, J-P., Humler, E. 2006. Trends and rhythms in global seafloor generation rate. Geochem. Geophys. Geosyst., 7,Q03011, doi:10.1029/2005GC001148.

Cogné, J.P., Humler, E., Courtillot, V., 2006. Mean age of oceanic lithosphere drives eustatic sea-level change since Pangea breakup. Earth Planet. Sci. Lett. 245, 115–122.

Crowley, J.W., Katz, R.F., Huybers, P., Langmuir, H.C., Sung-Hyun, P., 2015. Glacial cycles drive variations in the production of oceanic crust. Science 347(6227), 1237–1240.

Cruz, A.M., 2018. Integrated geological and geophysical studies applied to understanding the evolution of the Offshore Amazon Basin. PhD Thesis. Sorbonne Université, 223p.

Damuth, J., Embley, R., 1981. Mass transport processes on Amazon Cone: Western Atlantic Ocean. AAPG Bull. 65, 629–643.

Damuth, J.E., Flood, R.D., Kowsmann, R.O., Belderson, R.H. and Gorini, M.A., 1988. Anatomy and growth pattern of Amazon Deep-sea Fan revealed by long-range side-scan sonar (GLORIA) and high resolution seismic studies. AAPG Bulletin 72, 885–911.

Damuth, J., Kumar, N., 1975. Amazon Cone: morphology, sediments, age, and growth pattern. Geol. Soc. Am. Bull. 6, 863–878.

DeCelles, P.G., Ducea, M.N., Kapp, P., Zandt, G., 2009. Cyclicity in Cordilleran orogenic systems. Nat. Geosci. 2, 251–257.

de Silva, S.L., Riggs, N.R., Barth, A.P., 2015. Quickening the pulse: fractal tempos in continental arc magmatism. Elements 11,113–118.

Embry, S., Beauchamp, B., Dewing, K., Dixon, J., 2019. Episodic tectonics in the Phanerozoic succession of the Canadian High Arctic and the "10-million-year flood". in Piepjohn, K., Strauss, J.V., Reinhardt, L. & McClelland, W.C., eds.: Circum-Arctic Structural Events: Tectonic Evolution of the Arctic Margins and Trans-Arctic Links with Adjacent Orogens. Geological Society of America Special Paper 541. doi.org/10.1130/2018.2541(11).

Figueiredo, J.J.P., Zalán, P.V. and Soares, E.F., 2007. Bacia da Foz do Amazonas: Boletim de Geociencias da Petrobras, 15, 2, 299–309.

Friedrich, O., Norris, R.D., Erbacher, J., 2012. Evolution of middle to Late Cretaceous oceans—A 55 m.y. record of Earth's temperature and carbon cycle. Geology 40, 107–110.

Galeotti, S., Rusciadelli, G., Sprovieri, M., Lanci, L., Gaudio, A., Pekar, S., 2009. Sea-level control on facies architecture in the Cenomanian–Coniacian Apulian margin (Western Tethys): A record of glacio-eustatic fluctuations during the Cretaceous greenhouse? Palaeogeography Palaeoclimatology Palaeoecology 276, 196–205.

Gorini, C., Haq, U.B., dos Reis, A.T, Silva, C.G., Cruz, A.M., Soares, E., Grangeon, D., 2013. Late Neogene sequence stratigraphic evolution of the Foz do Amazonas Basin, Brazil. Terra Nova 26, 179–185.

Gornitz, V., Lebedeff, S., Hansen, J., 1992. Global sea-level trend in the past century. Science 215, 1611–1614.

Gradstein, F.M., Ogg, J.G., Schmitz, K., Ogg, G., 2012. The Geologic Time Scale 2012, vol. 2. Elsevier. 1144 p.

Gradstein, F.M., Ogg, J.G., Smith, A.G., 2004. A Geologic Time Scale 2004. Cambridge University Press, 589 p.

Haq, B.U., 2014. Cretaceous eustasy revisited. Glob. Planet. Change, 113, 44–58.

Haq, B.U., Hardenbol, J., Vail, P.R., 1987. Chronology of fluctuating sea levels since the Triassic. Science 235, 1156–1167.

Haq, B.U., Hardenbol, J., Vail, P.R., 1988. Mesozoic and Cenozoic chronostratigraphy and cycles of sea-level change. SEPM 42, 71–108.

Haq, B.U., Huber, B.T., 2016. Anatomy of a eustatic event during the Turonian (Late Cretaceous) hot greenhouse climate. Science China Earth Sciences 60, 20–29, doi: 10.1007/s11430-016-0166-y.

Hays, J.D., Imbrie, J., Schackleton, N.J., 1976. Variations in the Earth's orbit: Pacemaker of the ice ages. Science 194, 1121–1132.

Hilgen, F.J., 2010. Astronomical dating in the 19th century. Earth-Science Reviews 98, 65–80.

Hinnov, L.A., 2013. Cyclostratigraphy and its revolutionizing applications in the earth and planetary sciences. GSA Bulletin 125 (11/12), 1703–1734.

Hinnov, L.A., Hilgen, F., 2012. Cyclostratigraphy and Astrochronology. In Gradstein, F.M., Ogg, J.G., Schmitz, K., Ogg, G. (2012) (Ed.), The Geologic Time Scale 2012, Elsevier, vol. 2, Chapter 4, p. 63–83.

Huber, B.T., MacLeod, K.G., Watkins, D.K., Coffin, M.F., 2018. The rise and fall of the Cretaceous Hot Greenhouse climate. Global and Planetary Change 167, 1–23.

Huber, B.T., Norris, R.D., MacLeod, K.G., 2002. Deep-sea paleotemperature record of extreme warmth during the Cretaceous. Geology 30, 123–126.

Huybers, P., Langmuir, C., 2009. Feedback between deglaciation, volcanism and atmospheric CO2. Earth Planet. Sci. Lett. 286, 479–491.

Jacobs, D.K., Sahagian, D.L., 1993. Climate-induced fluctuations in sea level during nonglacial times. Nature 361, 710–712.

Jarvis, I., Lignum, J.S., Gröcke, D.R., Jenkyns, H.C., and Pearce, M.A., 2011. Black shale deposition, atmospheric CO2 drawdown, and cooling during the Cenomanian-Turonian Oceanic Anoxic Event. Paleoceanography 26, PA3201.

Huang, Z., Boyd, R., O'Connel, S., 1992. Upper Cretaceous cyclic sediments from hole 762C, Exmouth Plateau, Northwest Australia. In: Van Rad, U., Haq, B.U., et al. (Eds.), Proc. Ocean Drilling Program. Sci. Res, vol. 122, pp. 259–277.

Huber, B.T., MacLeod, K.G., Watkins, D.K., Coffin, M.F., 2018. The rise and fall of the Cretaceous Hot Greenhouse climate. Global and Planetary Change 167, 1–23.

Jenkyns, H.C., 2010. Geochemistry of oceanic anoxic events. Geochemistry, Geophysics, Geosystems 11, Q03004, doi:10.1029/2009GC002788.

Kominz, M.A., Browning, J.V., Miller, K.G., Sugarman, P.J., Minzintseva, S., Scotese, C.R., 2008. Late Cretaceous to Miocene sea-level estimates from the New Jersey and Delaware plain coreholes: an error analysis. Basin Research 20, 211–226.

Kutterolf, S., Jegen, M., Mitrovica, J.X., Kwasnitschka, T., Freundt, A., Huybers, P.J., 2012. A detection of Milankovitch frequencies in global volcanic activity. Geology 41, 227–230.

Laskar, J., 1990. The chaotic motion of the Solar System: a numerical estimate of the size of the chaotic zone. Icarus 88, 266–291.

Laskar, J., Fienga, A., Gastineau, M., Manche, H., 2011. La2010: a new orbital solution for the long term motion of the Earth. Astron. Astrophys. 532, A89. https://doi.org/10.1051/0004-6361/201116836.

Laskar, J., Robutel, P., Joutel, F., Gastineau, M., Correia, A.C.M., Levrard, B., 2004. A long-term numerical solution for the insolution quantities of the Earth. Astron. Astrophys. 428, 261–285.

Lees, J.A., Bown, P.R., 2005. Upper Cretaceous calcareous nannofossil biostratigraphy, ODP Leg 198 (Shatsky Rise, northwest Pacific Ocean). In: Bralower, T.J. Premoli Silva, I. Malone, M.J. (Ed.) Proceedings of the Ocean Drilling Program, Scientific Results, College Station, TX (Ocean Drilling Program), 198, 1–60, https://doi.org/10.2973/odp.proc.sr.198.114.2005.

Liu, Z., Huang, C., Algeo, T.J., Liu, H., Hao, Y., Du, X., Lu, Y., Chen, P., Guo, L., Peng, L., 2018. High-resolution astrochronological record for the Paleocene-Oligocene (66–23Ma) from the rapidly subsiding Bohai Bay Basin, northeastern China. Palaeogeogr. Palaeoclimatol. Palaeoecol. 510, 78–92.

MacLeod, K.G., Huber, B.T., Berrocoso, Á.J., Wendler, I., 2013. A stable and hot Turonian without glacial δ18O excursions is indicated by exquisitely preserved Tanzanian foraminifera. Geology 41, 1083–1086.

Mann, M.E., Lees, J.M., 1996. Robust estimation of background noise and signal detection in climatic time series. Clim. Change 33, 409–445.

Maslin, M., Mikkelsen, N., Vilela, C. and Haq, B.U., 1998. Sea-level and gas hydrate controlled catastrophic sediment failures of the Amazon Fan. Geology 26, 1107–1110.

Matos, R.M.D., 2000. Tectonic Evolution of the Equatorial South Atlantic. Atlantic Rift and Continental Margins 115, 331–354.

Matthews, R.K., 1984. Oxygen-isotopic record of ice-volume history: 100 million years of glacioeustatic fluctuations. AAPG Mem. 36, 97–107.

Mayer, H., Appel, E., 1999. Milankovitch cyclicity and rock-magnetic signatures of paleoclimatic changes in the Early Cretaceous Biancone Formation of the Southern Alps, Italy. Cretac. Res. 20, 189–214.

Mello, M.R., Koustsoukos, E.A.M., Hart, M.B., Brassell, S.C. and Maxwell, J.R., 1989. Late Cretaceous anoxic events in the Brazilian continental margin. Organic Geochemistry 14, 529–542.

Mello, M.R., Mosmann, R., Silva, S.R.P., Maciel, R.R., Miranda, F.P., 2001. Foz do Amazonas area: The last frontier for elephant hydrocarbon accumulations in the South Atlantic realm. In: M.W., Downey, J. C., Threet and W. A. Morgan, (ed.), Petroleum provinces of the twenty-first century. AAPG Memoir 74, p. 403–414.

Mello, M. R., Telnaes, N. and Maxwell, J. R., 1995. The hydrocarbon source potential in the Brazilian marginal basins: a geochemical and paleoenvironmental assessment. In: Huc, A.Y. (ed.), Paleogeography, Paleoclimate and Source Rocks. AAPG, Studies in Geology, 40, p. 233–272.

Meyers, S.R., 2014. Astrochon: An R Package for Astrochronology (Available at). cran.rproject.org/web/packages/astrochron/index.html.

Miller, K.G., Kominz, M.A., Browning, J.V.,Wright, J.D.,Mountain, G.S., Katz, M.E., Sugarman, P.J., Cramer, B.S., Christie-Blick, N., Pekar, S.F., 2005a. The Phanerozoic record of global sea-level change. Science 310, 1293–1298.

Miller, K.G., Lombardi, C.J., Browning, J.V., Schmelz, W.J., Gallegos, G, Mountain, G.S., Baldwin, K.E. 2018. Back to basics of sequence stratigraphy: Early Miocene and mid-Cretaceous examples from the New Jersey paleoshelf. Journal of Sedimentary Research 88, 148-176.

Miller, K.G., Wright, J.D., Browning, J.V., 2005b. Visions of ice sheets in a greenhouse world. Marine Geology 217, 215-231.

Müller, R.D., Sdrolias, M., Gaina, C., Steinberger, B., Heine, C., 2008. Long-term sea-level fluctuations driven by ocean basin dynamics. Science 319, 1357–1362.

Myers, K.J., Milton, N.J. 1996. Concepts and principles of sequence stratigraphy. In: Emery, D., Myers, K.J. (Eds.) Sequence Stratigraphy. Blackwell, Oxford, 11-44.

Navarro-Ramirez, J.P., Bodin, S., Heimhofer, U., Immenhauser, A., 2015. Record of Albian to early Cenomanian environmental perturbation in the eastern sub-equatorial Pacific. Palaeogeogr. Palaeoclimatol. Palaeoecol. 423, 122–137.

Paillard, D., Labeyrie, L., Yiou, P, 1996. Macintosch program performs timeseries analysis. Eos 77, 379.

Pälike, H., Laskar, J., Shackleton, N.J., 2004. Geologic constraints on the chaotic diffusion of the Solar System. Geology 32, 929–932.

Pälike, H., Norris, R.D., Herrle, J.O., Wilson, P.A., Coxall, H.K., Lear, C.H., Shackleton, N.J., Tripati, A.K., Wade, B.S., 2006. The Heartbeat of the Oligocene Climate System. Science 314, 1894–1898.

Paul, C.R.C., Lamolda, M.A., Mitchell, S.F., Vaziri, M.R., Gorostidi, A., Marshall, J.D., 1999. The Cenomanian-Turonian boundary at Eastbourne (Sussex, UK): a proposed European reference section. Palaeogeography, Palaeoclimatology, Palaeoecology 150, 83–121.

Perovano, R., Reis, A.T. dos, Silva, C.G., Vendeville, B.C., Gorini, C., Oliveira, V. De, and Araújo, É.F. da S., 2009, O Processo de Colapso Gravitacional da Seção Marinha da Bacia da Foz do Amazonas - Margem Equatorial Brasileira: Revista Brasileira de Geofíca, v. 27, no. 3, p. 459–484.

Posamentier, H.W., Vail, P.R., 1988. Eustatic controls on clastic deposition II—sequence and systems tract models. In: Wilgus, C.K., Ross, C.A., Posamentier, H. (Eds.), Sea- level Changes: An Integrated Approach. SEPM Special Publication, 42, 125–154.

Ray, D.C., van Buchem, F.S.P, Baines, G., Davies, A., Gréselle, B., Simmons, M.D., Robson, C., 2019. The magnitude and cause of short-term eustatic Cretaceous sea-level change: A synthesis. Earth-Science Reviews 197, 102901.

Reis, A.T., Araújo, E., Silva, C.G., Cruz, A.M., Gorini, C., Droz, L., Migeon, S., Perovano, R., King, I., and Bache, F., 2016, Effects of a regional décollement level for gravity tectonics on late Neogene to recent large-scale slope instabilities in the Foz do Amazonas Basin, Brazil: Marine and Petroleum Geology, doi: 10.1016/j.marpetgeo.2016.04.011.

Reis, A. T., Perovano, R., Silva, C.G., Vendeville, B.C., Araujo, E., Gorini, C., and Oliveira, V., 2010. Two-scale gravitational collapse in the Amazon Fan: a coupled system of gravity tectonics and mass-transport processes. J. Geol. Soc. London 167, 593–604, doi: 10.1144/0016-76492009-035.

Sames, B., Wagreich, M., Wendler, J.E., Haq, B.U., Conrad, C.P., Melinte-Dobrinescu, M.C., Hu, X., Wendler, I., Wolfgring, E., Yilmaz, I.Ö., Zorina, S.O., 2016. Short-term sea-level changes in a greenhouse world—A view from the Cretaceous. Palaeogeography, Palaeoclimatology, Palaeoecology 441, 393–411.

Schulz, M., Schäfer-Neth, C., 1998. Translating Milankovitch climate forcing into eustatic fluctuations via thermal deep water expansion: a conceptual link. Terra Nova 9, 228–231.

Schlanger, S.O., Jenkyns, H.C., 1976. Cretaceous oceanic anoxic events: causes and consequences. Geol. Mijnb. 55, 179–184.

Silva, C.G., Araújo, E.F.S., Reis, A.T., Perovano, R., Gorini, C., Vendeville, B.C., Albuquerque, N.C. 2010. Megaslides in the Foz do Amazonas Basin, Brazilian Equatorial Margin. In: Submarine Mass Movements and Their Consequences (D.C. Mosher, R.C. Shipp, L. Moscardelli, J.D. Chaytor, C.D.P. Baxter, H.J. Lee and R. Urgeles, eds). Adv. Nat. Technol Hazards 28, 581– 591. Springer‐Verlag, New York.

Silva, S.R.P., Maciel, R.R., Severino, M.C.G., 1999. Cenozoic tectonics of Amazon Mouth Basin. Geo-Marine Letters 18, 256–262.

Simmons, M.D., 2012. Sequence Stratigraphy and Sea-Level Change. In: Gradstein, F.M., Ogg, J.G., Schmitz, M.D., Ogg, G.M. (Eds.) The Geologic Time Scale 2012, v.1, pp. 239–267.

Simmons, M.D., Miller, K.G., Ray, D.C., Davies, A., van Buchem, F.S.P, Gréselle, B., in press. Phanerozoic eustasy. In: Gradstein, F.M., Ogg, J.G., Schmitz, M.D., Ogg, G.M. (Eds.) The Geologic Time Scale 2020, v.x, pp. xxx–xxx.

Sprovieri, M., Sabatino, N., Pelosi, N., Batenburg, S.J., Coccioni, R., Iavarone, M., Mazzola, S., 2013, 2013. Late Cretaceous orbitally-paced carbon isotope stratigraphy from the Bottaccione Gorge (Italy). Palaeogeogr. Palaeoclim. Palaeoecol. 379–380, 81–94.

Stoll, H.M., Schrag, D.P., 1996. Evidence for glacial control of rapid sea level changes in the Early Cretaceous. Science 272, 1771–1774.

Stoll, H.M., Schrag, D.P., 2000. High-resolution stable isotope records from the Upper Cretaceous rocks of Italy and Spain: Glacial episodes in a greenhouse planet? Geological Society of America Bulletin 112, 308–319.

Strasser, A., Pittet, B., Hillgärtner, H., Pasquier, J.B., 1999. Depositional sequences in shallow carbonate-dominated sedimentary systems: concepts for a high-resolution analysis. Sedimentary Geology 128, 201–221.

Strasser, A., Hillgärtner, H., Hug, W., Pittet, B., 2000. Third-order depositional sequences reflecting Milankovitch cyclicity. Terra Nova 12, 303–311.

Thomson, D.J., 1982. Spectrum estimation and harmonic analysis. IEEE Proc.70, 1055–1096.

Tsikos, H., Karakitsios, V., van Breugel, Y., Walsworth-Bell, B., Bombardière, L., Petrizzo, M.R., Sinninghe Damsté, J.S., Schouten, S., Erba, E., Premoli Silva, I., Farrimond, P., Tyson, R.V., Jenkyns, H.C., 2004. Organic carbon deposition in the Cretaceous of the Ionian Basin, NW Greece: The Paquier event (OAE1b) revisited. Geological Magazine 141, 401–416.

Vail, P.R.,Mitchum, R.M., Todd, J.R.G.,Widmier, J.M., Thompson, S., Sangree, J.B., Bubb, J.N., Hatlelid,W.G., 1977. In: Payton, C.E. (Ed.), Seismic stratigraphy and global changes of sea level: Seismic Stratigraphy – Applications to Hydrocarbon Exploration. Mem. Am. Ass. Pertol. Geol. 26, pp. 49–212.

Wagreich, M., Lein, R., Sames, B., 2014. Eustasy, its controlling factors, and the limn-eustatic hypothesis – concepts inspired by Eduard Suess. Austrian Journal of Earth Sciences 107, 115-131.

Weedon, G.P., Coe, A.L., Gallois, R.W., 2004. Cyclostratigraphy, orbital tuning and inferred productivity for the type Kimmeridge Clay (Late Jurassic), Southern England. Journal of the Geological Society 161, 655–666.

Wendler, J.E., Wendler, I., Vogt, C., Kuss, J. 2016. Link between cyclic eustatic sea-level change and continental weathering: evidence for aquifer-eustasy in the Cretaceous. Palaeogeography, Palaeoclimatology, Palaeoecology 441, 430-437.

Wilson, P.A., Norris, R.D., 2001. Warm tropical ocean surface and global anoxia during the mid-Cretaceous period. Nature 412, 425–429.

Wolfram, L.C., Weinberg, R.F., Nebel, O., Hamza, K., Hasalová, P., Míková, J., Becchio, R., 2019. A 60-Myr record of continental back-arc differentiation through cyclic melting. Nat. Geosci. 12, 215–219.

Wu, H., Zhang, S., Jiang, G., Hinnov, L., Yang, T., Li, H., Wan, X. and Wang, C., 2013. Astrochronology of the Early Turonian–Early Campanian terrestrial succession in the Songliao Basin, northeastern China and its implication for long-period behavior of the Solar System. Palaeogeogr. Palaeoclimatol. Palaeoecol. 385, 55–70.

Figures and tables captions

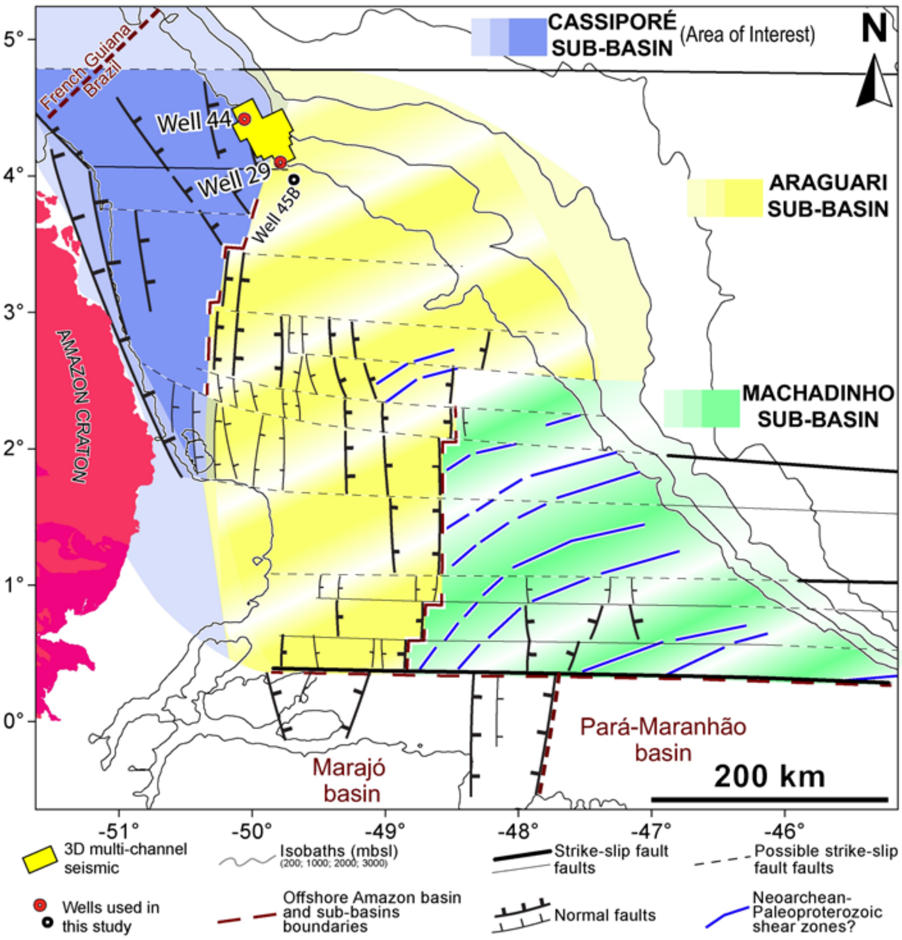

Figure 1: Simplified structural framework of the Foz do Amazonas Basin based on an integrated study of seismic reflection and potential field data (Cruz, 2018). The three studied petroleum wells 1-APS-29-AP, 1-APS-44-AP and 1-APS-45B-AP (indicated as 29, 44 and 45B). Well 45B is used only for biostratigraphic data because it captures only the top of the Limoeiro Fm (see Fig. SI-7).

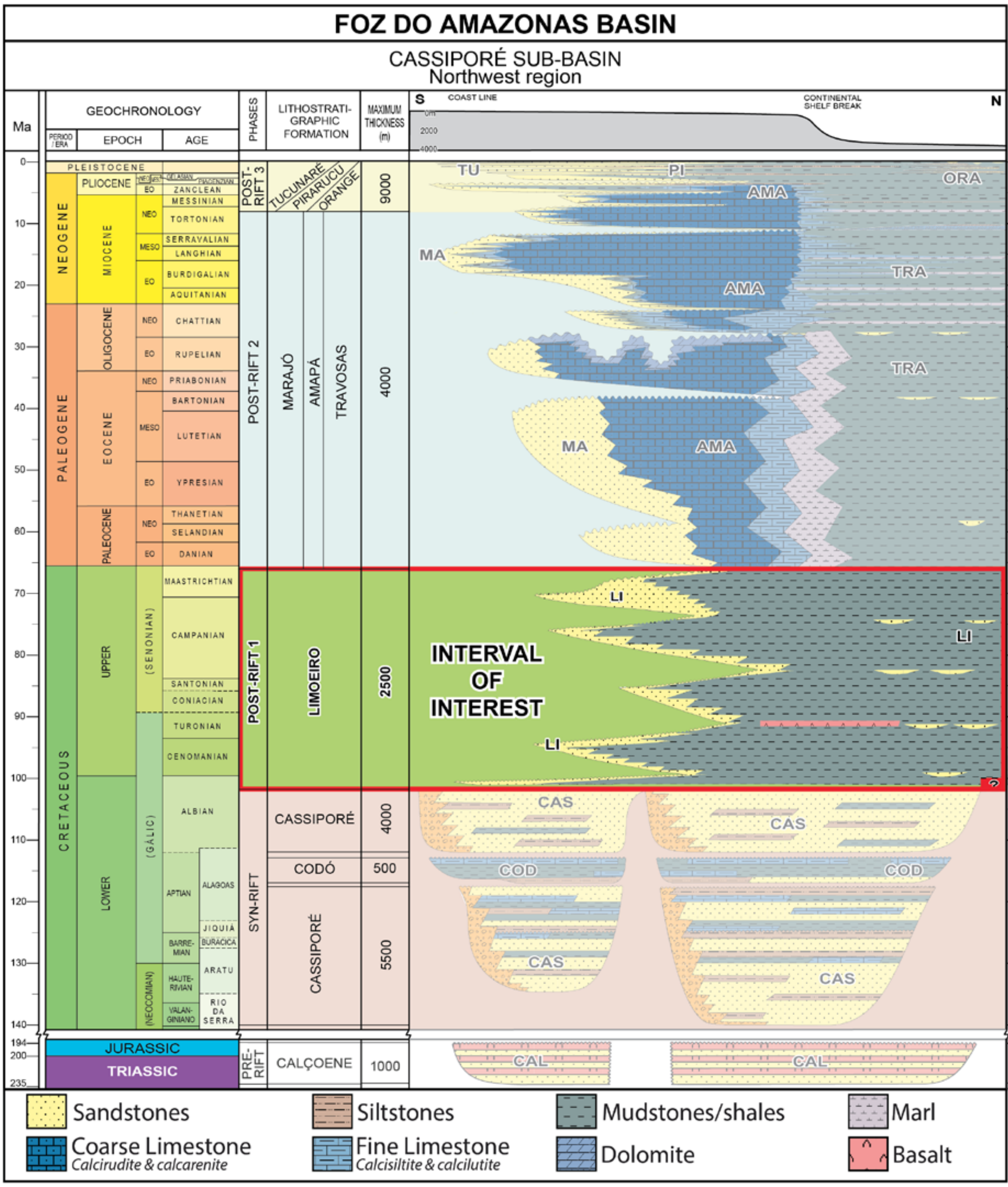

Figure 2: Stratigraphic chart of the Cassiporé Sub-basin (NW Amazon Margin); red box highlights the stratigraphic interval investigated in this study, dashed lines indicate the three post-rift megasequences (modified from Cruz, 2018). Late Cretaceous to Triassic based on Figueiredo et al. (2007), and age calibration of Limoeiro Fm according to the present study.

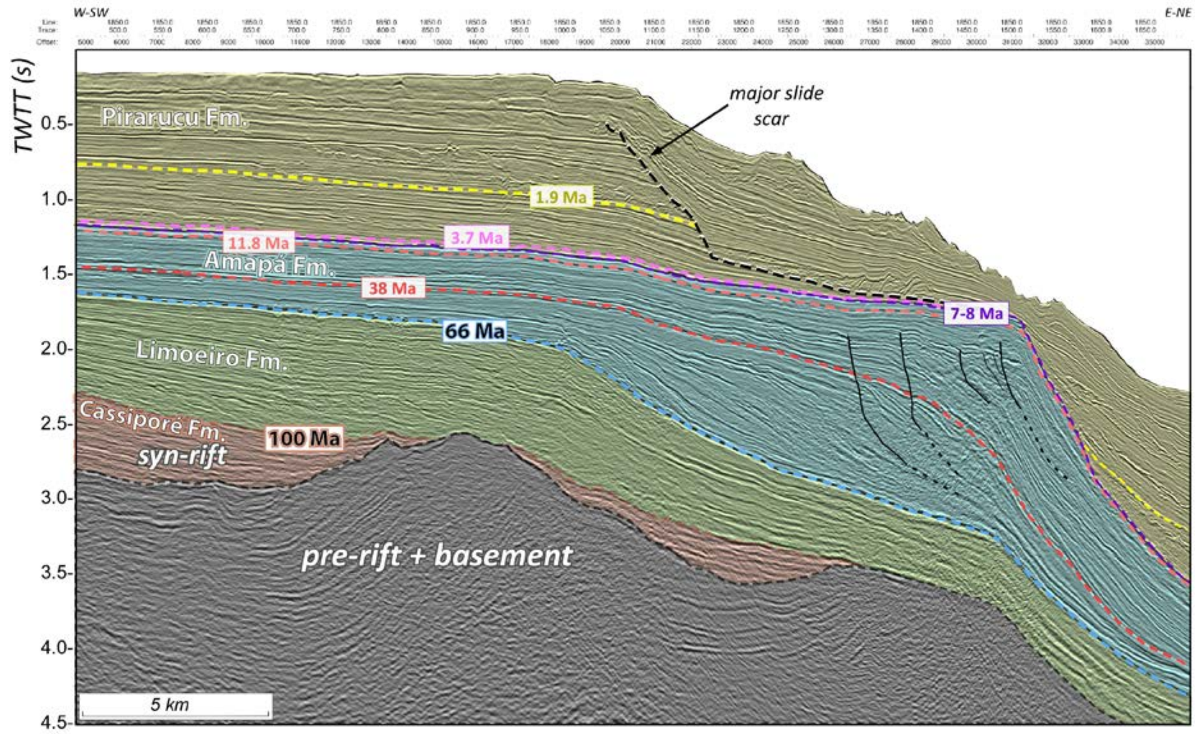

Figure 3: Interpreted seismic profile across NW Amazon Margin (Cassiporé Sub-basin) showing the basement and pre-rift strata, overlain by syn-rift Cassiporé Fm (orange), and post-rift Limoeiro (green), Amapá (blue) and Pirarucu (yellow) Formations (modified from Baker et al., 2015; Cruz, 2018) .

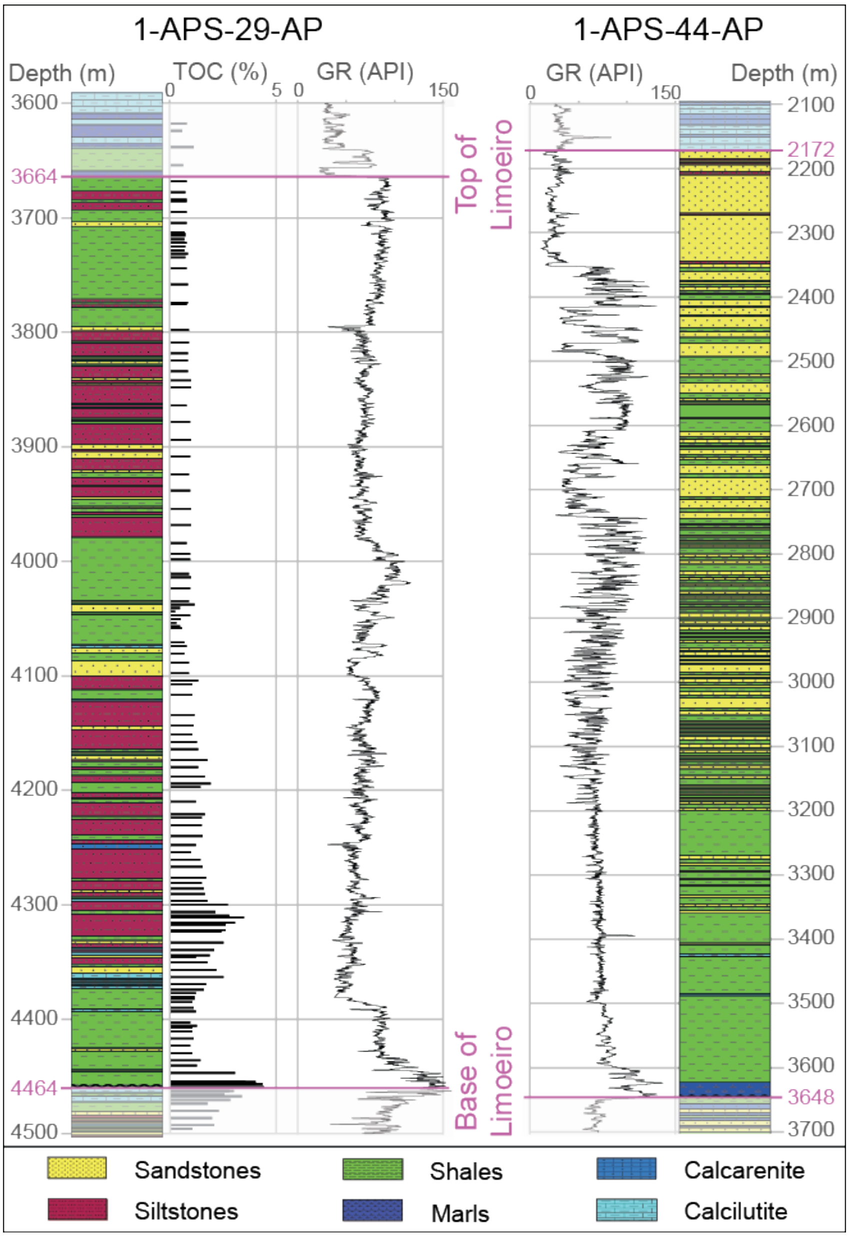

Figure 4: Lithostratigraphy and gamma-ray (GR) log data of the Limoeiro Fm in Wells 29 and 44, and Total Organic Carbon (TOC) data in Well 29.

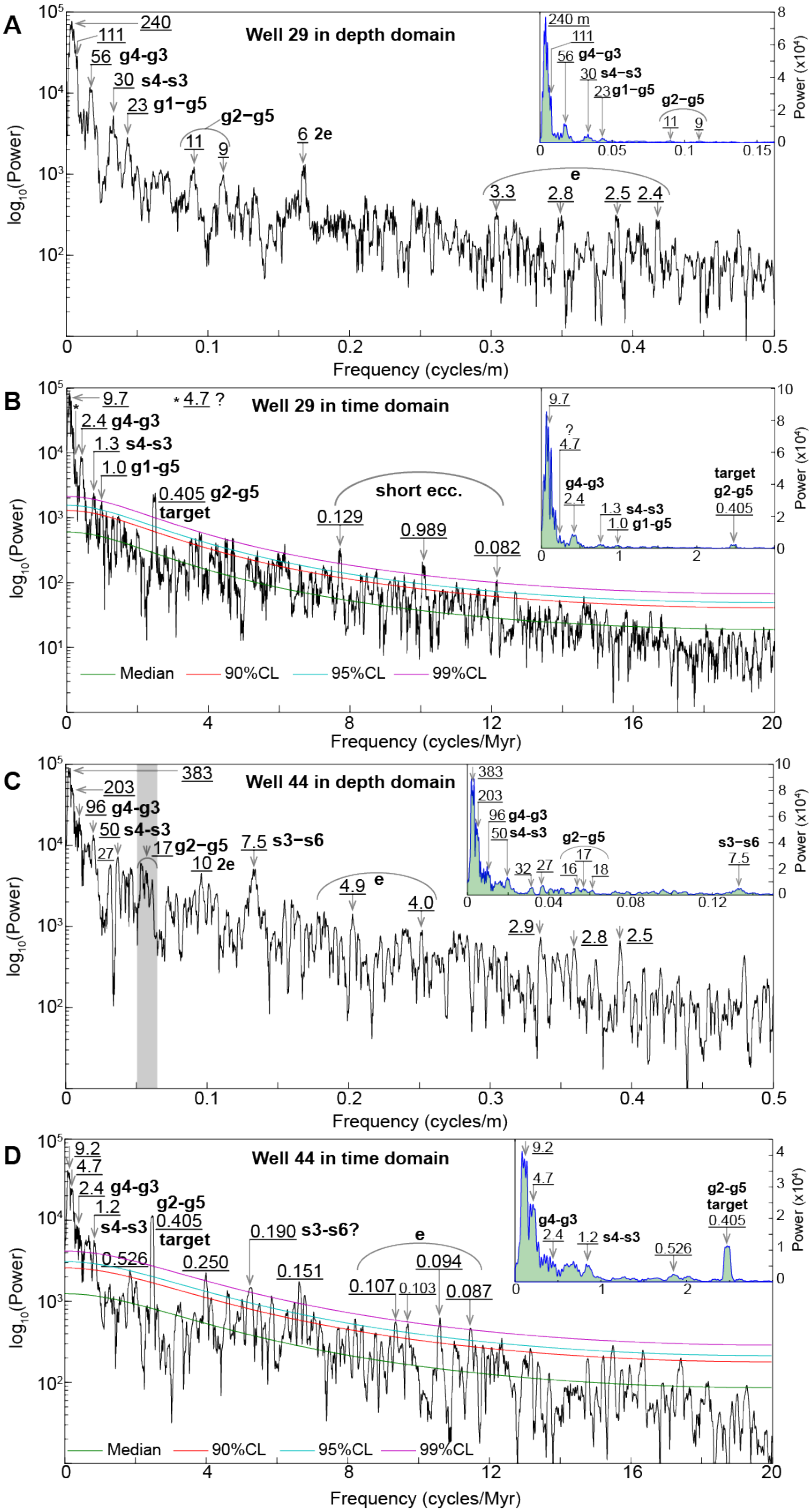
A
Well 29 in depth domain
log10(Power)
Frequency (cycles/m)
240
111
56 g4-g3
30 s4-s3
23 g1−g5
g2−g5
11
9
6 2e
e
3.3
2.8
2.5
2.4
240 m
Power (x10⁴)
B
Well 29 in time domain
9.7
4.7 ?
2.4 g4-g3
1.3 s4-s3
1.0 g1-g5
0.405 g2-g5
target
short ecc.
0.129
0.989
0.082
Median
90%CL
95%CL
99%CL
Frequency (cycles/Myr)
C
Well 44 in depth domain
383
203
96 g4-g3
50 s4-s3
27
17 g2−g5
10 2e
7.5 s3−s6
4.9
4.0
2.9
2.8
2.5
32
16
18
D
Well 44 in time domain
9.2
4.7
2.4 g4-g3
1.2
s4-s3
g2-g5
0.405
target
0.526
0.250
0.190 s3-s6?
0.151
0.107
0.103
0.094
0.087

Figure 5: 2π-MTM power spectra of untuned (A and C) and tuned (B and D) GR data of the Limoeiro Fm equivalent interval in Well 29 (3400-4580 m) and Well 44 (2045-3725 m). **(A)** Spectrum of 35% weighted average detrended GR data in Well 29. *Inset*: Spectrum in a linear scale power axis together with truncated frequency axis at 0.16 cycles/m. **(B)** Spectrum of the raw GR data in Well 29. *Inset*: Spectrum in a linear scale power axis together with truncated frequency axis at 3 cycles/Myr. **(C)** Spectrum of 35% weighted average detrended GR data in Well 44. *Inset*: Spectrum in a linear scale power axis together with truncated frequency axis at 0.15 cycles/m. **(D)** Spectrum of 35% weighted average detrended GR data in Well 44. *Inset*: Spectrum in a linear scale power axis together with truncated frequency axis at 3 cycles/m.

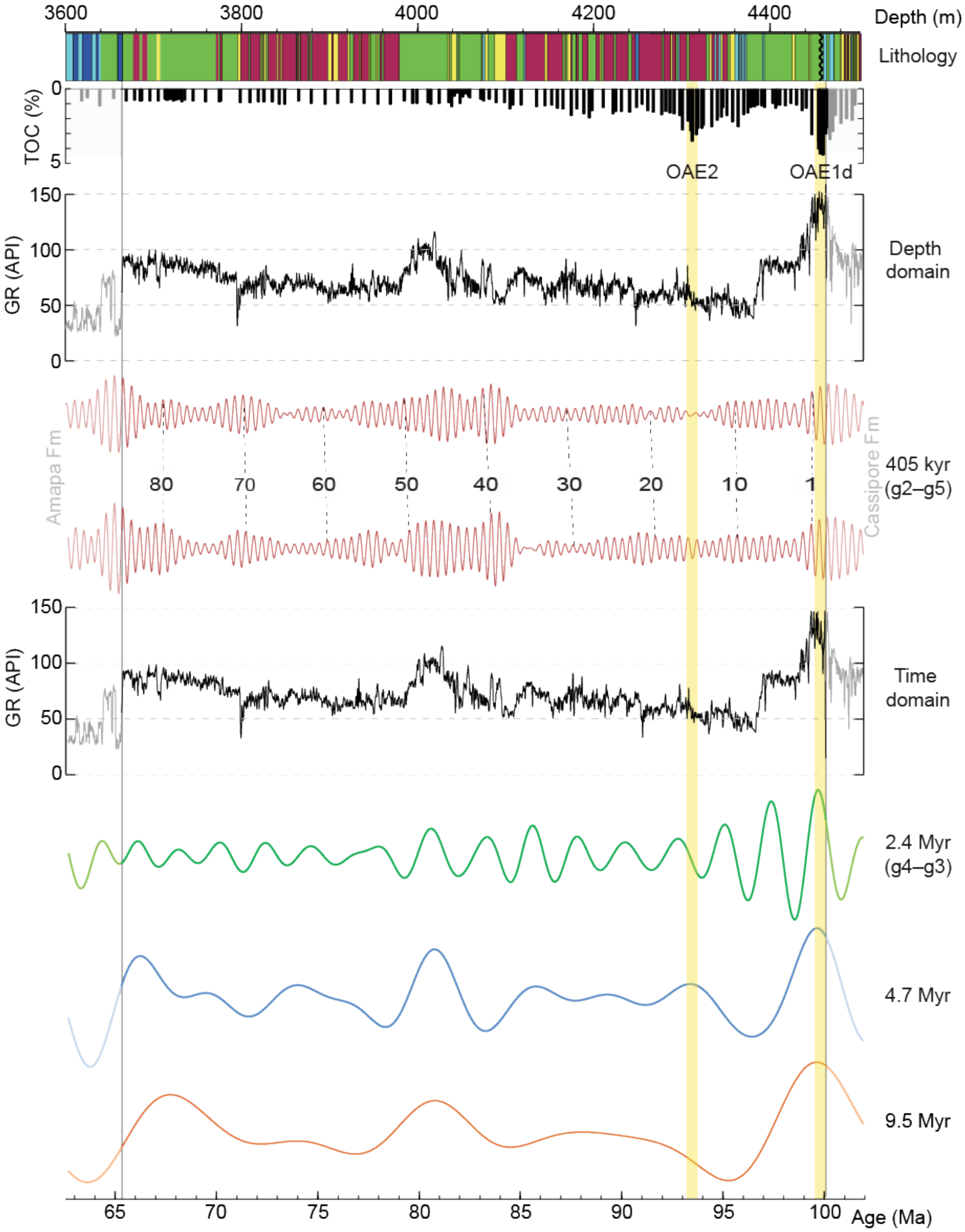

Figure 6: Astronomical age model of the Limoeiro Fm in Well 29 along with bandpass filtering of long-period Milankovitch cycles (405 kyr, 2.4, 4.7 and 9.5 Myr orbital cycles).

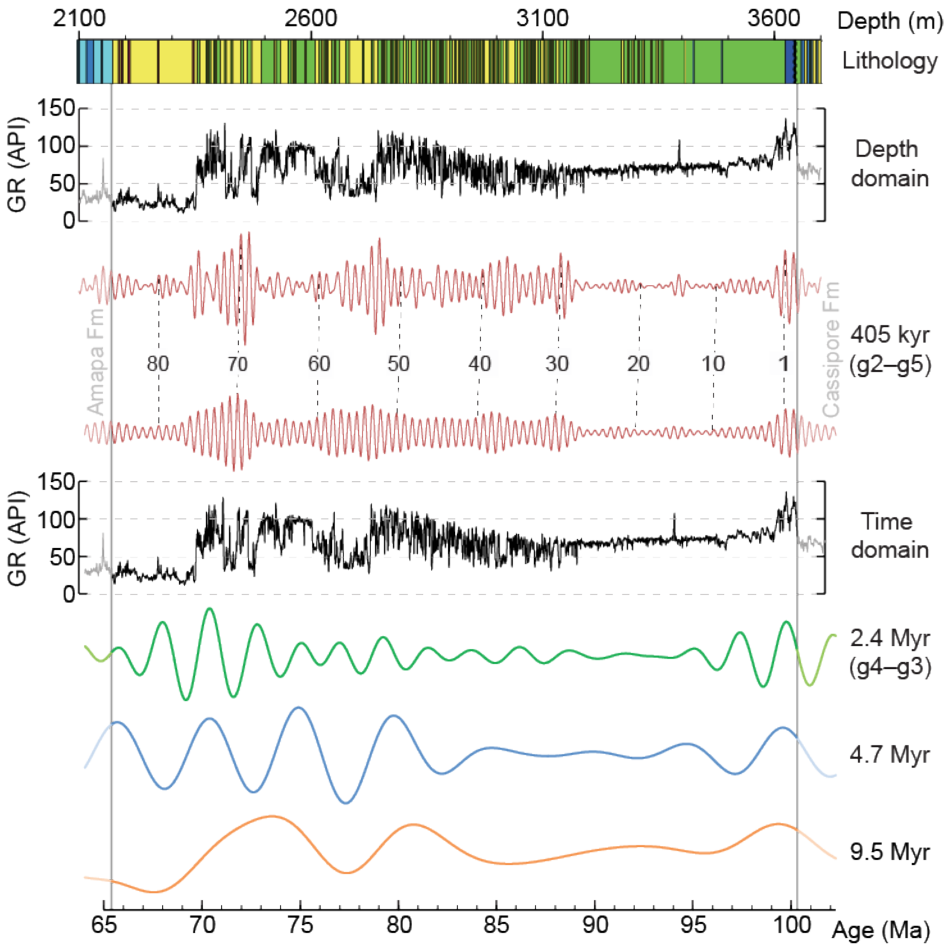

Figure 7: Astronomical age model of the Limoeiro Fm in Well 44 along with bandpass filtering of long-period Milankovitch cycles (405 kyr, 2.4, 4.7 and 9.5 Myr orbital cycles).

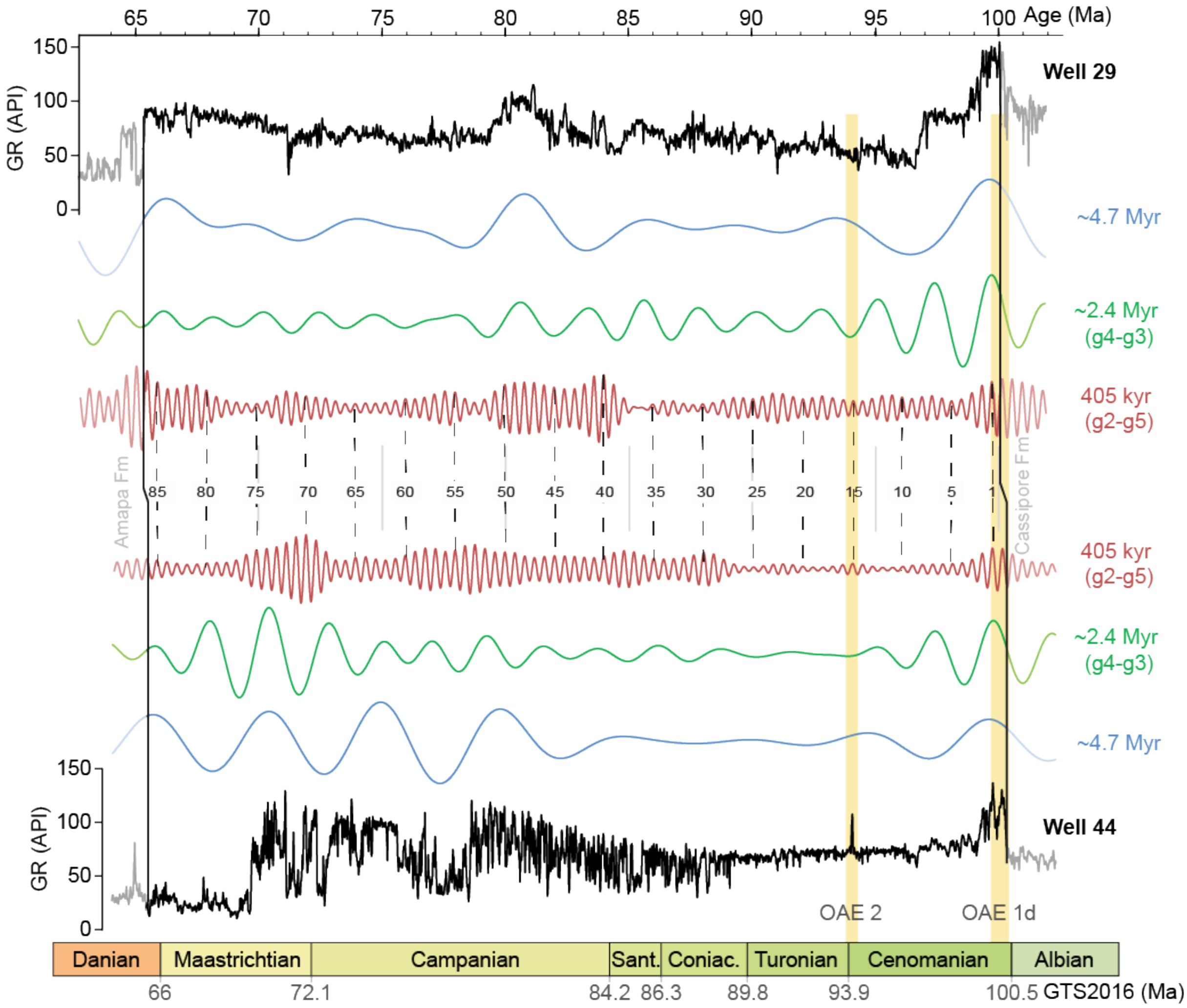

Figure 8: Correlation of astronomical age models of the Limoeiro Fm in Well 29 versus Well 44, along with bandpass filtering of long-period Milankovitch cycles (405 kyr, 2.4, 4.7 Myr orbital cycles).

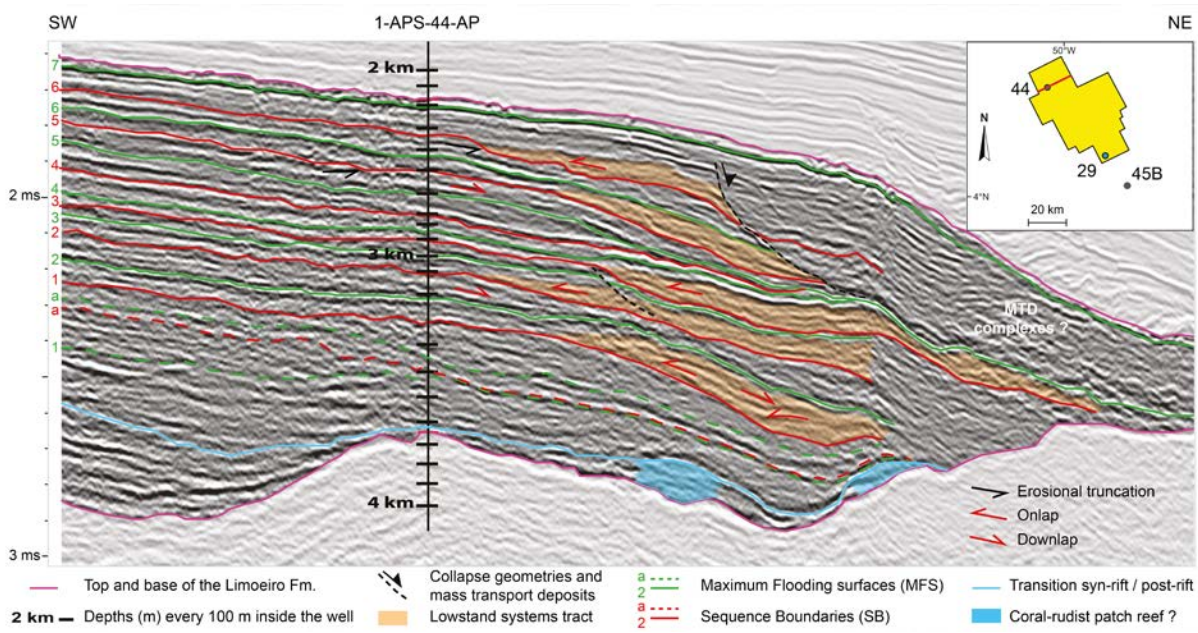

Figure 9: Seismic interpretation of the Limoeiro Fm in the inline crossing Well 44 from 3D seismic data.

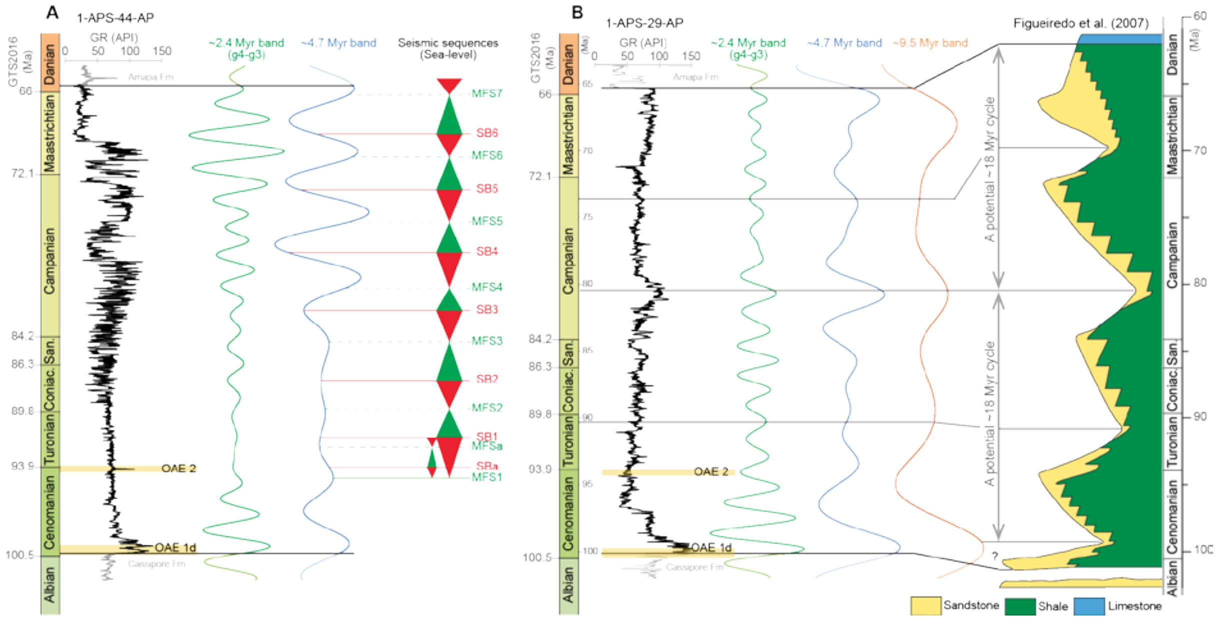

Figure 10: Correlation of 4.7 and 9.5 Myr orbitally related cycles inferred from GR cyclostratigraphy, and main SL sequences inferred from seismic data and previous studies. **(A)** Correlation of 4.7 Myr orbital cycles with seismically detected second-order SL sequences in Well 44. **(B)** Correlation of 9.5 Myr orbital cycles in Well 29 with the main SL sequences that compose the Limoeiro Fm (Figueiredo et al., 2007).

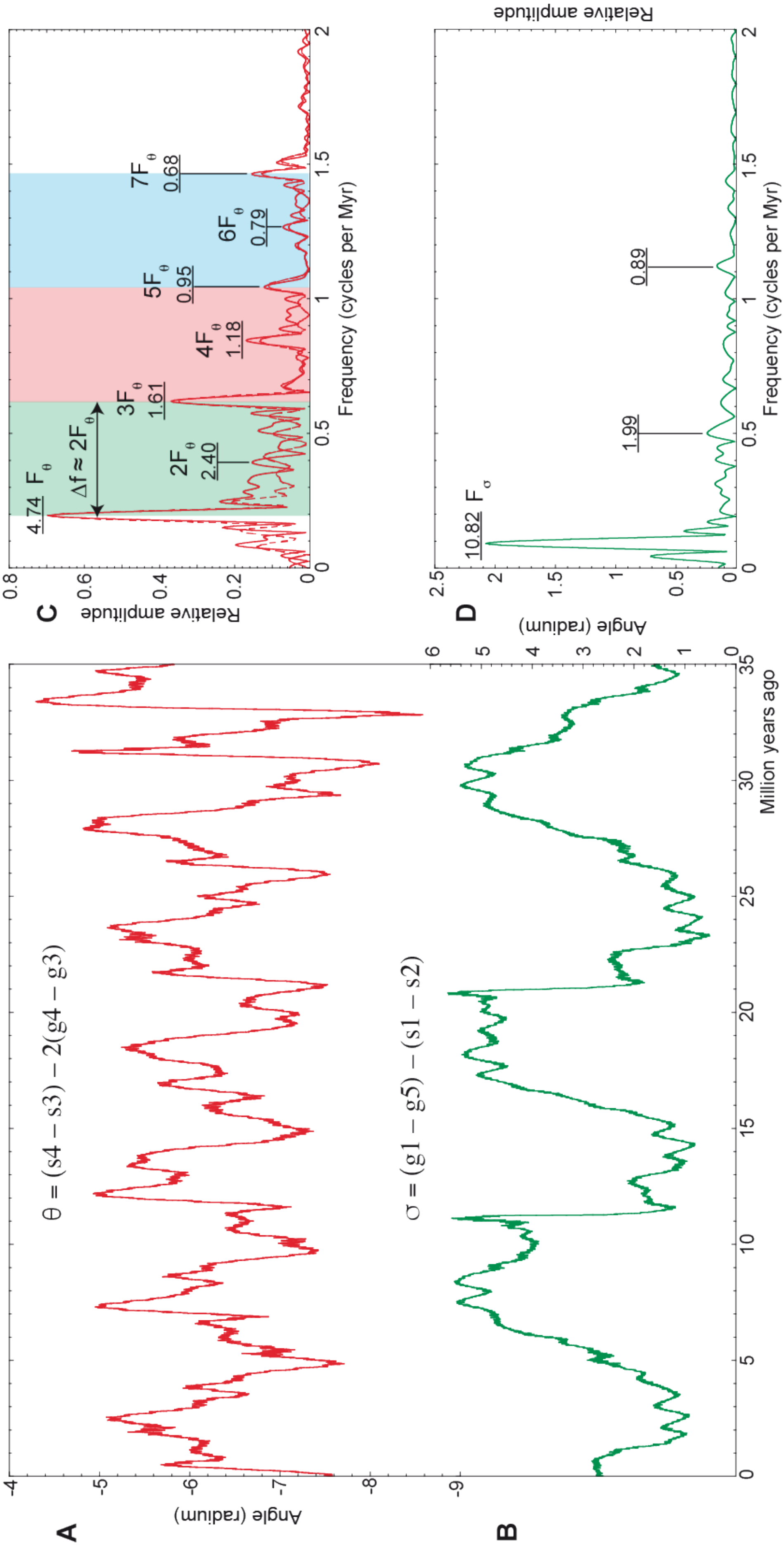
A
B
C
D
θ = (s4 – s3) – 2(g4 – g3)
σ = (g1 – g5) – (s1 – s2)
Angle (radium)
Million years ago
Relative amplitude
Frequency (cycles per Myr)
4.74 Fθ
Δf ≈ 2Fθ
2Fθ 2.40
3Fθ 1.61
4Fθ 1.18
5Fθ 0.95
6Fθ 0.79
7Fθ 0.68
10.82 Fσ
1.99
0.89

Figure 11: Harmonic analysis of the resonant arguments θ and σ over the past 35 Ma. **(A)** Variations of θ. **(B)** Variations of σ. **(C)** 2pi-MTM amplitude spectrum of θ. Fundamental libration frequency 'Fθ' and its harmonics (3Fθ, 5Fθ and 7Fθ) are indicated by shaded areas. **(D)** 2pi-MTM amplitude spectrum of σ, the main peak represents the fundamental libration frequency 'Fσ'.

Earth's orbital parameters	Interfering terms (periods in kiloyear)	Resulting long periods (associated to θ or σ)
Climatic precession	$p + g_3 \approx 19.1$ $p + g_4 \approx 18.9$	$g_4 - g_3 \approx 2.4$ Myr (θ)
	$p + g_1 \approx 23.1$ $p + g_5 \approx 23.6$	$g_1 - g_5 \approx 1$ Myr (σ)
	$p + g_4 \approx 18.94$ $p + g_{n6} \approx 19.29$	$g_4 - g_{n6} \approx 1.6$ Myr (θ)
	$p + g_3 \approx 19.07$ $p + g_{n7} \approx 19.29$	$g_3 - g_{n7} \approx 4.7$ Myr (θ)
Obliquity	$p + s_1 \approx 28.8$ $p + s_2 \approx 29.8$	$s_1 - s_2 \approx 0.9$ Myr (σ)
	$p + s_3 \approx 40.8$ $p + s_4 \approx 39.4$	$s_4 - s_3 \approx 1.2$ Myr (θ)
	$p + \nu_{10} \approx 41.5$ $p + s_3 \approx 40.8$	$s_3 - \nu_{10} \approx 2.4$ Myr (θ)
	$p + \nu_{20} \approx 40.06$ $p + s_4 \approx 39.4$	$s_4 - \nu_{20} \approx 2.4$ Myr (θ)
Eccentricity	$g_4 - g_5 \approx 94.9$ $g_3 - g_5 \approx 98.8$	$g_4 - g_3 \approx 2.4$ Myr (θ)
	$g_4 - g_2 \approx 123.7$ $g_3 - g_2 \approx 130.8$	$g_4 - g_3 \approx 2.4$ Myr (θ)
	$g_2 - g_5 \approx 405$ $(g_2 - g_5) + (g_4 - g_3) \approx 346$	$g_4 - g_3 \approx 2.4$ Myr (θ)
	$g_2 - g_5 \approx 405$ $(g_2 - g_5) - (g_4 - g_3) \approx 490$	$g_4 - g_3 \approx 2.4$ Myr (θ)
	$g_4 - g_3 \approx 2361$ ($2F_\theta$) $g_4 - g_{n6} \approx 1624$ ($3F_\theta$)	$g_3 - g_{n6} \approx 4.7$ Myr (θ)
	$g_4 - g_3 \approx 2361$ ($2F_\theta$) $g_3 - g_{n7} \approx 4700$ (F_θ)	$g_4 - g_{n7} \approx 4.7$ Myr (θ)

Table 1: Possible interfering terms of Earth's orbital parameters (climatic precession, obliquity and eccentricity) and the resulting long-period cyclicities associated with the main resonant arguments θ = 2(g4 – g3) − (s4 – s3) and σ = (g1 – g5) – (s1 – s2). 'p' is the Earth's axial precession (present-day value: 50.4758 arcsec/yr, Laskar et al., 2004) and 'g_i' and 's_i' are the secular frequencies as in Table SIII-1. 'Fθ' is the fundamental libration frequency related to the argument θ (see 'Section 5.2' for detail). ν_{10} and ν_{20} are two higher order terms

of s3 – (g4 – g3) and s4 – (g4 – g3), respectively. g_{n6} and g_{n7} are $g_3 - F\theta$ and $g_3 + F\theta$, respectively.

Order	Suborder	Mean period (Myr)	Causal mechanism	Astronomy
First	Longer	250-300*	Tectonic, galactic?	Radial motion?
	Shorter	91*	Tectonic, galactic?	
Second	Longer	36*	Tectonic, galactic?	Vertical motion?
	Medium-2	**18**	Tectonic, Milankovitch?	
	Medium-1	9.5	Milankovitch?	**Eccentricity-Obliquity?**
	Shorter	**4.7**	**Milankovitch**	**Eccentricity-Obliquity**
Third	Longer	2.4	Milankovitch	Eccentricity (g4-g3)
	Shorter	1.2	Milankovitch	Obliquity (s4-s3)
Fourth		0.405	Milankovitch	Eccentricity (g2-g5)
Fifth	Longer	0.173	Milankovitch	Obliquity
	Shorter	0.1	Milankovitch	Eccentricity
Sixth	Longer	0.04	Milankovitch	Obliquity
	Shorter	0.020	Milankovitch	Precession

Table 2: Updated SL sequence hierarchy and causal mechanisms. Bold text indicates the updates. The remaining are as in a review by Boulila et al. (2011, 2018a). * Phanerozoic mean periodicity.

Earth's orbital parameters	Interfering terms (periods in kiloyear)	Resulting long periods (associated to θ or σ)
Climatic precession	$p + g_3 \approx 19.1$ $p + g_4 \approx 18.9$	$g_4 - g_3 \approx 2.4$ Myr (θ)
	$p + g_1 \approx 23.1$ $p + g_5 \approx 23.6$	$g_1 - g_5 \approx 1$ Myr (σ)
	$p + g_4 \approx 18.94$ $p + g_{n6} \approx 19.29$	$g_4 - g_{n6} \approx 1.6$ Myr (θ)
	$p + g_3 \approx 19.07$ $p + g_{n7} \approx 19.29$	$g_3 - g_{n7} \approx 4.7$ Myr (θ)
Obliquity	$p + s_1 \approx 28.8$ $p + s_2 \approx 29.8$	$s_1 - s_2 \approx 0.9$ Myr (σ)
	$p + s_3 \approx 40.8$ $p + s_4 \approx 39.4$	$s_4 - s_3 \approx 1.2$ Myr (θ)
	$p + \nu_{10} \approx 41.5$ $p + s_3 \approx 40.8$	$s_3 - \nu_{10} \approx 2.4$ Myr (θ)
	$p + \nu_{20} \approx 40.06$ $p + s_4 \approx 39.4$	$s_4 - \nu_{20} \approx 2.4$ Myr (θ)
Eccentricity	$g_4 - g_5 \approx 94.9$ $g_3 - g_5 \approx 98.8$	$g_4 - g_3 \approx 2.4$ Myr (θ)
	$g_4 - g_2 \approx 123.7$ $g_3 - g_2 \approx 130.8$	$g_4 - g_3 \approx 2.4$ Myr (θ)
	$g_2 - g_5 \approx 405$ $(g_2 - g_5) + (g_4 - g_3) \approx 346$	$g_4 - g_3 \approx 2.4$ Myr (θ)
	$g_2 - g_5 \approx 405$ $(g_2 - g_5) - (g_4 - g_3) \approx 490$	$g_4 - g_3 \approx 2.4$ Myr (θ)
	$g_4 - g_3 \approx 2361$ $(2F_\theta)$ $g_4 - g_{n6} \approx 1624$ $(3F_\theta)$	$g_3 - g_{n6} \approx 4.7$ Myr (θ)
	$g_4 - g_3 \approx 2361$ $(2F_\theta)$ $g_3 - g_{n7} \approx 4700$ (F_θ)	$g_4 - g_{n7} \approx 4.7$ Myr (θ)

Order	**Suborder**	**Mean period (Myr)**	**Causal mechanism**	**Astronomy**
First	Longer	250-300*	Tectonic, galactic?	Radial motion?
	Shorter	91*	Tectonic, galactic?	
Second	Longer	36*	Tectonic, galactic?	Vertical motion?
	Medium-2	**18**	Tectonic, Milankovitch?	
	Medium-1	9.5	Milankovitch?	**Eccentricity-Obliquity?**
	Shorter	**4.7**	**Milankovitch**	**Eccentricity-Obliquity**
Third	Longer	2.4	Milankovitch	Eccentricity (g4-g3)
	Shorter	1.2	Milankovitch	Obliquity (s4-s3)
Fourth		0.405	Milankovitch	Eccentricity (g2-g5)
Fifth	Longer	0.173	Milankovitch	Obliquity
	Shorter	0.1	Milankovitch	Eccentricity
Sixth	Longer	0.04	Milankovitch	Obliquity
	Shorter	0.020	Milankovitch	Precession